

# Tracers of Discs and Winds around Intermediate and High Mass Young Stellar Objects

S.L. Lumsden<sup>1</sup>, H.E. Wheelwright<sup>1,2</sup>, M.G. Hoare<sup>1</sup>, R.D. Oudmaijer<sup>1</sup> and J.E. Drew<sup>3</sup>

<sup>1</sup> Department of Physics and Astronomy, University of Leeds, Leeds LS2 9JT, UK

<sup>2</sup> Max Planck Institute for Radio Astronomy, 53121 Bonn, Germany

<sup>3</sup> Department of Physical Sciences, University of Hertfordshire, Hatfield, Hertfordshire, AL10 9AB, UK

*Email* – [s.l.lumsden@leeds.ac.uk](mailto:s.l.lumsden@leeds.ac.uk)

25 February 2024

## ABSTRACT

We present a study of the kinematical properties of a small sample of nearby near-infrared bright massive and intermediate mass young stellar objects using emission lines sensitive to discs and winds. We show for the first time that the broad ( $\sim 500\text{km s}^{-1}$ ) symmetric line wings on the HI Brackett series lines are due to Stark broadening or electron scattering, rather than pure Doppler broadening due to high speed motion. The results are consistent with the presence of a very dense circumstellar environment. In addition, many of these lines show evidence for weak line self-absorption, suggestive of a wind or disc-wind origin for that part of the absorbing material. The weakness of the self-absorption suggests a large opening angle for such an outflow. We also study the fluorescent  $1.688\mu\text{m}$  FeII line, which is sensitive to dense material. We fitted a Keplerian disc model to this line, and find reasonable fits in all but one case, in agreement with previous finding for classical Be stars that fluorescent iron transitions are reasonable disc tracers. Overall the picture is one in which these stars still have accretion discs, with a very dense inner circumstellar environment which may be tracing either the inner regions of a disc, or of a stellar wind, and in which ionised outflow is also present. The similarity with lower mass stars is striking, suggesting that at least in this mass range they form in a similar fashion.

**Key words:** accretion discs; line: profiles; stars: wind, outflows; stars: pre-main-sequence; stars: formation

## 1 INTRODUCTION

There are well recognised and long-standing difficulties in describing high-mass star formation as a simple scaled-up version of the low-mass case (eg Kahn 1974, Shu, Adams & Lizano 1987). Radiation pressure is sufficient to prevent further accretion once fusion commences in the stellar core, preventing the formation of a star much more massive than  $20 M_{\odot}$  in the simple low mass theory. This led to alternative models of high-mass star formation being suggested (e.g. Bonnell, Vine & Bate 2004, Stahler, Palla & Ho 2000, McKee & Tan 2003) which can generally be subdivided into two groups: those that overcome the mass limit by forming massive stars through competitive accretion in dense cluster cores and those that look for a working version of the scaled-up low-mass star formation paradigm, essentially overcoming the pressure from the star through self-shielded disc accretion. Dynamical models of disc accretion around massive stars are now being produced which appear to overcome the mass limit (eg Krumholz et al. 2009 who model the formation of a  $40 M_{\odot}$  star, and Kuiper et al. 2010 who find

radiation pressure is not an efficient means of preventing disc accretion even in very massive stars). Such models are therefore currently favoured as the most likely. This agrees with limited observational data, where infrared interferometry has revealed disk-like structures (eg. Kraus et al. 2010). However we still have little direct evidence for accretion in a large sample of young massive stars.

The obvious alternative method to apply to a large sample is to look for kinematical evidence of a disc. The  $2.3\mu\text{m}$  CO first overtone rotation-vibration emission is believed to mostly arise in an accretion disc in young stars (eg, Carr 1989, Chandler, Carlstrom & Scoville 1995, Bik & Thi 2004, Blum et al. 2004, Wheelwright et al. 2010, Davies et al. 2010). The physical conditions required for its origin are characteristic of the properties of a disc that is self-shielded (temperature in the range  $1000\text{--}5000\text{K}$ , density greater than  $10^{10}\text{cm}^{-3}$ ), since it allows for the presence of molecular gas relatively near the exciting star. Generally, the spectra of objects studied in this way have been better fitted by a disc model than other alternatives. However not all mas-

sive young stellar objects show CO bandhead emission (eg Porter, Drew & Lumsden 1998). There are many reasons why this might be, but the most plausible are that the accretion rate may simply be too low to give detectable emission, or, there may be too little column density to create the self-shielding condition required in the disc to prevent the intense UV flux from more massive stars reaching the mid-plane and destroying the CO. The CO bandhead is also relatively complex to interpret without high signal-to-noise data (eg Wheelwright et al) because of the blending of the multiple rotational transitions that make up the  $v = 2 - 0$  vibrational transition.

Another complicating factor in high mass stars is that other emission mechanisms are also likely to be present. The most obvious of these is a stellar wind which can clearly be seen in at least some massive young stellar objects (eg Drew, Bunn & Hoare 1993, Bunn, Drew & Hoare 1995, the models presented by Sim, Drew & Long 2005, and see Section 3.2). A powerful stellar wind is a fairly natural consequence of a high accretion rate in any hot star system. Winds in young stars are usually traced by recombination lines of common elements, particularly hydrogen and helium (eg Simon et al. 1983 and Persson et al. 1984 at moderate spectral resolution, and Bunn, Drew and Hoare 1995 at high enough resolution to fully sample the line profiles). These lines can also be excited in nebular gas and in a disc as well. An ideal study should combine tracers sensitive to the winds as well as those that sample density and temperature and ionisation ranges more typical of an accretion disc in order to clearly distinguish the origin of the emission. Therefore we need a transition that is only strongly excited at the higher densities seen in circumstellar discs around young stellar objects (eg  $n \gg 10^6 \text{ cm}^{-3}$ ).

Fortunately, there are other similar well studied situations from which we can draw likely candidates. For example, spectra of both active galactic nuclei (eg Baldwin et al 2004) and classical Be stars (Zorec et al. 2007) show fluorescent  $\text{Fe}^+$  emission consistent with an origin in a disc. It is not seen in ordinary nebular gas (eg as in an HII region: see, for example, Lumsden & Puxley 1996). FeII emission straddles the boundary between where CO emission might still arise (neutral material) and ionised material since its ionisation potential is only 7.9eV, with  $\text{Fe}^{2+}$  having an ionisation potential of 16.2eV. Carciofi & Bjorkman (2006) have successfully modelled the origin of this emission in Be star disks from an origin in the shielded material near the disk mid-plane. Accretion discs around young stars are likely to have additional opacity due to dust, but a similar partially ionised zone will exist within them.

Fluorescent excitation typically occurs when an atom/ion is irradiated by either UV continuum or Lyman series photons. The excited atom/ion cascades back down to the ground state, leading to transitions that would not typically be seen from the standard recombination process. The optical FeII lines have been well studied and modelled in both active galaxies and Be stars (eg Baldwin et al. 2004; Carciofi & Bjorkman 2006) but there are also infrared transitions that are more suitable for studying heavily embedded young stellar objects. In particular there are two strong lines near  $1.6\mu\text{m}$  (eg see the spectrum of  $\eta$  Carina in Hamann et al. 1994), of which the transition at  $1.6877808\mu\text{m}$  is both in a region of good atmospheric transmission, and near enough

in wavelength to the HI Br11 line that both can be compared without the need to worry about differential extinction. The  $1.6877808\mu\text{m } c^4\text{F}_9 - z^4\text{F}_9$  transition arises from an upper level 6.2eV above the ground state (Johansson 1978) and is likely to be pumped by  $\text{Ly}\alpha$  in situations just such as we are seeking (the dense ionised/neutral boundary) as discussed by Johansson & Letokhov (2007). Previous observations (Porter et al. 1998) indicate this particular line may be relatively common in massive young stellar objects, and more prevalent there than in lower mass objects (Hamann & Persson 1992).

The aim of this paper therefore is straightforward. We have observed a small sample of eight intermediate and high mass young stellar objects with sufficient spectral resolution to resolve the kinematics of the line emission in both FeII and HI recombination lines for the first time. The bulk of this sample have near and/or mid-infrared interferometric data available, allowing plausible limits to be placed on the inclination of the system and the size of any infrared emitting region in a disc. The comparison of both FeII and HI tracers is ideal for testing whether the FeII samples a different emission region from the HI recombination lines. The sample is therefore ideal for testing the value of the FeII line as a disc tracer, as well as expanding on the use of HI lines as studied previously (eg Bunn et al 1995) to those present in the  $H$  band. Our work presents a velocity resolved study of the higher Brackett series members 11-4 and 12-4 for the first time.

In section 2 we discuss the sample and the observations made, in Section 3 we discuss the observational results together with some simple model fits to our data and in Section 4 we sum up the evidence as to which features might be the best kinematical tracers of discs or winds around young massive stars.

## 2 OBSERVATIONS

The data were acquired on the nights of 24 and 25 June 2000 and 7 and 8 July 2001 using the facility near infrared spectrometer CGS4 on UKIRT. We used the echelle grating and 300mm camera with a one pixel wide slit. Due to anamorphic distortion within the instrument the spatial scale along and across the slit vary. The effective size of a pixel with this setup is 0.4 arcseconds across the slit, and 0.91 arcseconds along it. The measured spectral resolution from an arc calibration line was  $12 \text{ km s}^{-1}$ . The slit was oriented at the default north-south position angle. We observed two separate wavelength ranges for all of our targets, from approximately  $1.636\text{--}1.648\mu\text{m}$  in order to detect the  $1.6411725\mu\text{m}$  Br12 and  $1.6440018\mu\text{m } a^4\text{F}_9 - a^4\text{D}_7$  [FeII] lines, and  $1.679\text{--}1.691\mu\text{m}$  to detect the  $1.6811164\mu\text{m}$  Br11 and  $1.6877808\mu\text{m } c^4\text{F}_9 - z^4\text{F}_9$  FeII lines. We also observed the  $2.159\text{--}2.173\mu\text{m}$  range in order to measure  $2.166127\mu\text{m } \text{Br}\gamma$  for five of the targets. All wavelengths are in vacuum, and hereafter all wavelengths are truncated to three decimal places. All eight of the main targets are known massive YSOs or Herbig Ae/Be stars. Some basic properties of these are given in Table 1. Where possible we have derived inclinations from near or mid-infrared interferometry. For GL 490 we instead use results from mm CO interferometric measurements, and for S106 IRS we rely on models of the velocity structure. Where

Object	Distance (kpc)	Spectral type	Luminosity( $L_{\odot}$ )	$A_V$ (mag)	Inclination	$v_{LSR}$ (kms $^{-1}$ )
BD+40°4124/V1685 Cyg	$\sim 1^1$	B3V <sup>2</sup>		3.1 <sup>3</sup>	40 – 50° <sup>4</sup>	$\sim 8^5$
GL 490	$\sim 1^6$		2000 <sup>6</sup>	42 <sup>7</sup>	$\sim 30^{\circ 8}$	$-14^9$
M17SW IRS1	1.3/2.1 <sup>14</sup>	O9V <sup>15</sup>		17 <sup>16</sup>	76° <sup>15</sup>	$\sim 17^{17}$
M8E	1.25 <sup>10</sup>		20000 <sup>11</sup>	39 <sup>8</sup>	$\sim 20^{\circ 12}$	$\sim 11^{13}$
MWC 297	0.25 <sup>18</sup>	B1.5V <sup>18</sup>		8 <sup>18</sup>	5° <sup>19</sup> , < 40° <sup>20</sup> , 15° <sup>21</sup>	2 – 20 <sup>18</sup>
MWC 349A	1.7 <sup>22</sup>		60000 <sup>23</sup>	9 <sup>23</sup>	> 70° <sup>24</sup>	10 <sup>25</sup>
S106 IRS	0.5 – 1.7 <sup>26</sup>	O7.5V <sup>26</sup>		13.6 <sup>27</sup>	$\sim 75^{\circ 28}$	$\sim 5^{29}$
VV Ser	0.2 – 0.6 <sup>30</sup>	B6V <sup>2</sup> /B9V <sup>31</sup>		$\sim 3^{31}$	$\gtrsim 80^{\circ 32}$	$\sim 10^{33}$

**Table 1.** literature. 1: van den Ancker, de Winter & Tjin A Djie (1998); 2: Hernandez et al. (2004); 3: Oudmaijer, Busfield & Drew (1997), van den Ancker, Wesselius & Tielens (2000); 4: Eisner et al. (2003, 2004); 5: Fuente et al. (1990) from NH<sub>3</sub>; 6: Schreyer et al. (2002); 7: Willner et al. (1982); 8: Schreyer et al. (2006); 9: Waterlout & Brand (1989) from molecular gas (CO); 10: Prisinzano et al. (2005) assuming it is at the same distance as the resolved stellar cluster found in M8; 11: Thronson, Loewenstein & Stokes (1979); 12: Linz et al. (2009); 13: Bunn et al. (1995) from the star and Simon et al. (1984) from CO; 14: Estimates vary from 1.3kpc (Hanson, Howarth & Conti 1997) using spectral parallaxes to 2.1kpc (eg Hoffmeister et al. 2008) using photometric methods – we adopt the latter; 15: Follert et al. (2010); 16: Porter et al. (1998); 17: Bunn et al. (1995) from the star, Lada (1976) from CO; 18: Drew et al. (1997); 19: Alonso-Albi et al. (2009); 20: Acke et al. (2008); 21: Malbet et al. (2007); 22: Meyer, Nordsieck & Hoffman (2002); 23: Cohen et al. (1985); 24: Danchi, Tuthill & Monier (2001); 25: Gordon et al. (2001); 26: Schneider et al. (2007), we adopt the further distance, which their analysis shows results in the given spectral type; 27: van den Ancker et al. (2000); 28: Hippelein & Muench (1981), Solf & Carsenty (1982); 29: Bunn et al. (1995); 30: Montesinos et al. (2009); 31: Pontoppidan et al. (2007); 32: Eisner et al. (2003); 33: Corcoran & Ray (1997).

required the tabulated luminosities have been modified from the original references to take account of revised distances. For sources where an accurate spectral type can be inferred we have given that. For those where only a bolometric luminosity exists (generally the most heavily embedded) we have quoted that instead. All of these sources were chosen to be bright enough at  $H$  to be observable with CGS4. In addition, we observed the planetary nebula NGC 7027 and the yellow hypergiant IRC +10420 for calibration purposes. NGC 7027 provided a check of our wavelength calibration, since its velocity is known to a greater degree of accuracy than most of our target stars. IRC +10420 was observed as it is a known FeII emitter in the optical, and hence provides a check of our line identification. The sample is not in any sense complete or statistically representative of massive YSOs as a whole.

All the sources are sufficiently compact that they could be observed by nodding the telescope such that the sources remained on the slit (the measured beam separation is 22 arcseconds). We observed standard stars to provide crude flux calibration and correct for atmospheric absorption features in addition to observations of the targets. The standard stars were chosen to have a range of spectral type from G6V through to O9V. This provided enough range to enable us to correct for the observed Brackett line absorption in the standards themselves. Cooler stars were not used since they have many other spectral features in the wavelength ranges observed, and in practice we used the hottest standard available for any target. The Brackett line absorption in the standard was interpolated over to remove it. This gives good though not perfect correction: Br11 in particular may be affected by poor correction in the standard star since the line lies near the edge of the spectrum (cf Figure 1). There are some hints that the Br11 and Br12 line profiles differ in some objects (eg BD+40°4124, Figure 1), but the difficulty in correcting adequately for the instrumental response and interpolation of Br11 in the standard star makes it impossible to be sure these are real. We therefore do not use Br11 in our analysis. For Br12 and Br $\gamma$  the interpolation process

is far more secure, and is certainly adequate to define weak line wings.

A standard reduction procedure was adopted for all of the data discussed here. The projected image of the slit on the array is curved. This was corrected for using the trace of a bright arc line as a model. This procedure was checked for reliability using fainter night sky lines present on each individual exposure. Each frame was also checked to ensure that no velocity shifts were apparent, again using the night sky lines. Where such shifts were seen the data were realigned using the centroid of the night sky line.

Both of the beams were extracted from the data after correction for spectral distortion with wavelength. The typical extraction is 6 spatial pixels (or 4.5 arcseconds) to encompass the full image of the spectrum as seen on the array. The telescope was slightly defocused to correct for problems caused by the order sorting filter present in CGS4, which utilises a circular variable filter (CVF). This imposes a wavelength dependent transmission pattern on the spectra that contains both a high frequency component (approximately one resolution element) and a lower frequency component where the CVF response declines away from the centre of the observed wavelength range, giving lower transmission and signal-to-noise near the edges of the spectrum. The high frequency component also varies slightly with spatial position. The best correction is achieved if both object and atmospheric standard star have the same point spread function (PSF), so that the pattern divides out during the flux calibration. The easiest way to ensure this with CGS4 was to smear the PSF slightly for both. The data from the separate beams were treated individually since the CVF pattern is seen to vary at the few % level between the two beams.

The array was stepped six times across two pixels in order to fully sample the resolution element, and reduce the impact of bad pixels. These individual frames must be interleaved to give the final data and it is possible that any of sky transmission, atmospheric seeing or the position of the object in the narrow slit can change between frames. This is corrected for by looking for appropriate periodicity in the final spectra (ie a pattern repeating every 3 pixels) which

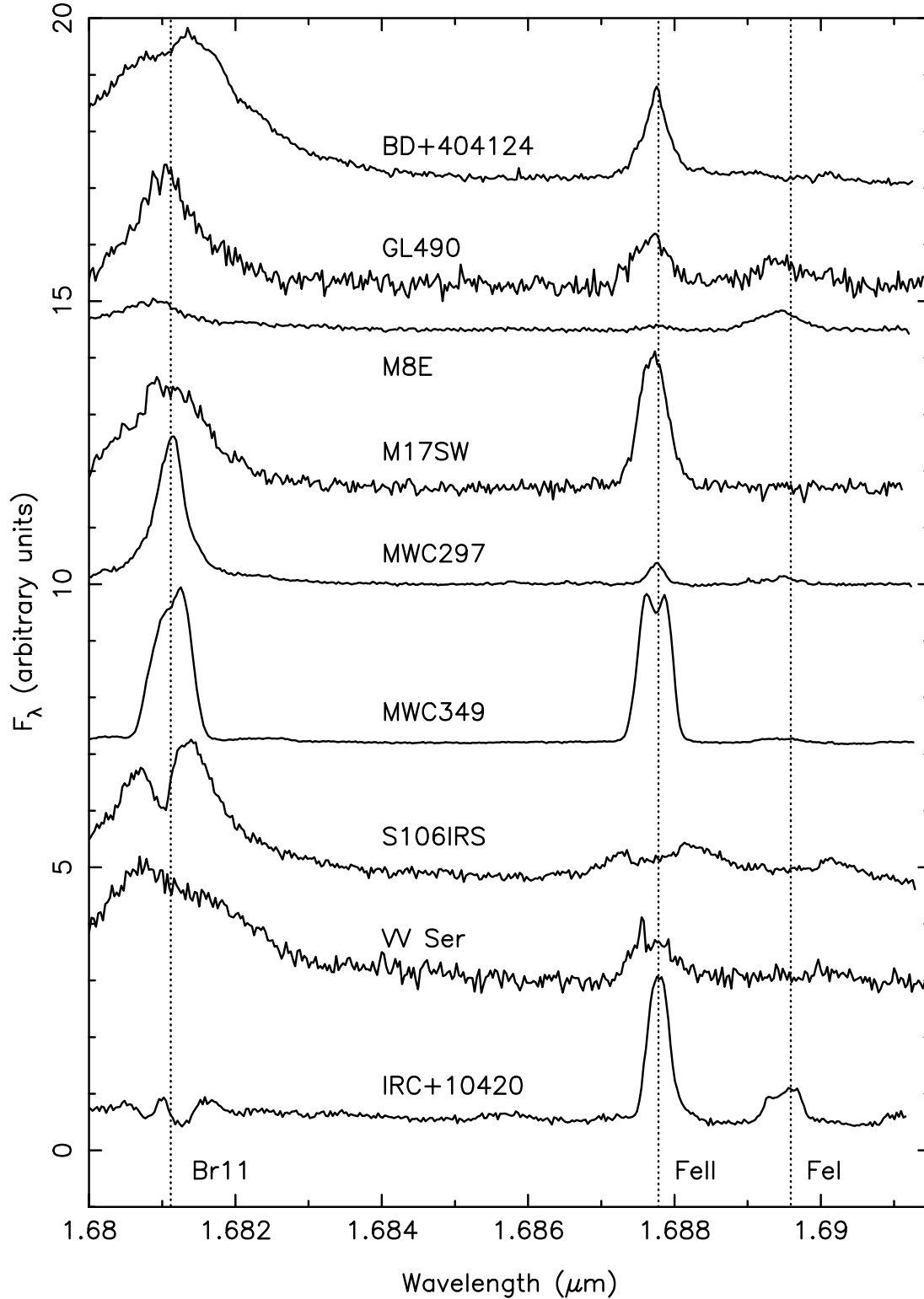


**Figure 1.** Spectra of the eight target stars and of the known FeII emitter IRC+10420 in the wavelength range showing HI Br11 1.681 $\mu\text{m}$  and the 1.688 $\mu\text{m}$   $z^4\text{F}_9\text{--}c^4\text{F}_9$  FeII line. Both the FeII line and HI Br11 rest wavelengths are indicated by the dotted lines, and the previously unidentified feature we associate with FeI is also shown. The spectra are presented in the rest frame after correction for their published  $v_{\text{LSR}}$  values for easier comparison.

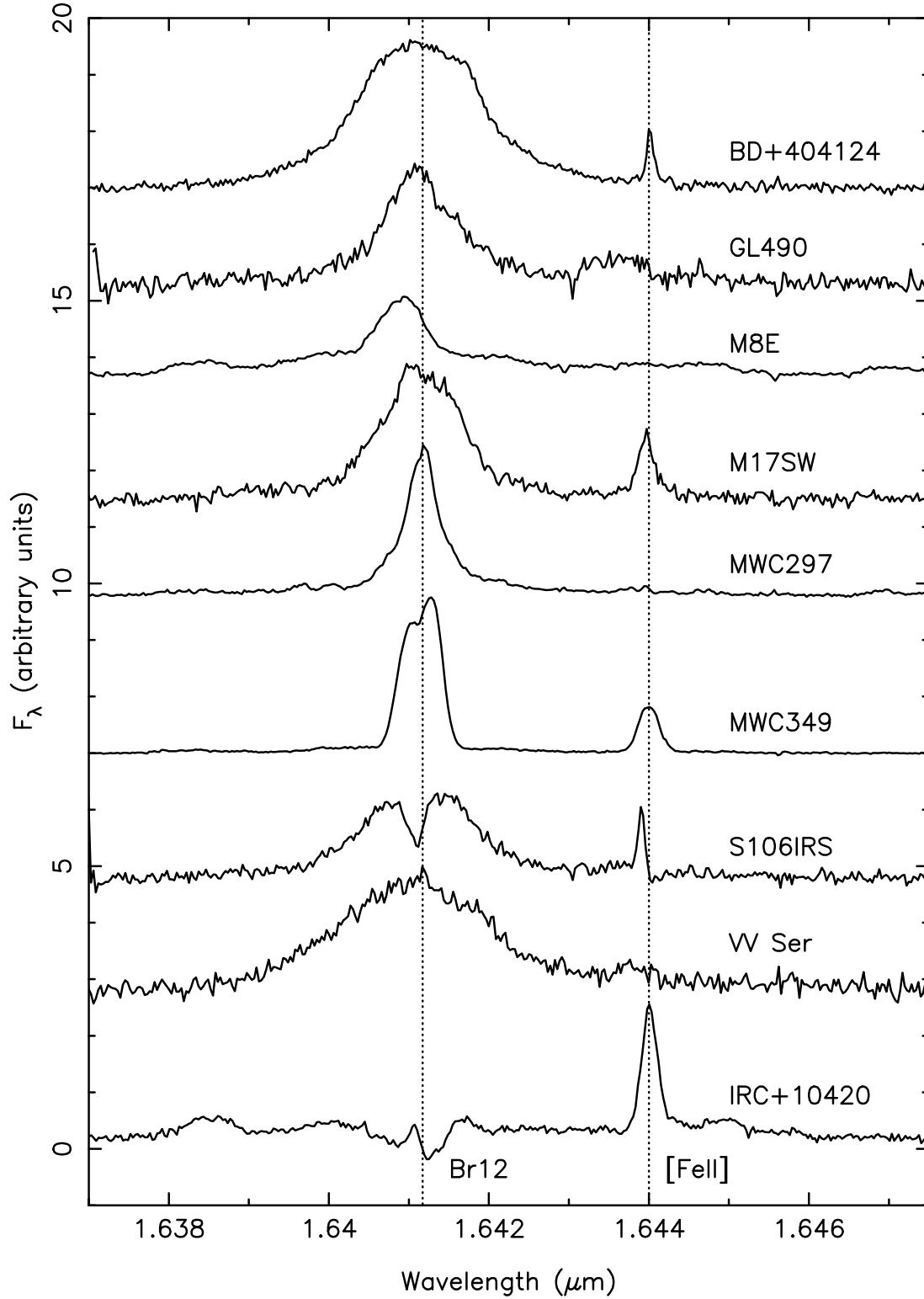


**Figure 1** – *continued* Spectra of the eight target stars and of the known FeII emitter IRC+10420 in the wavelength range showing HI Br12 1.641 $\mu\text{m}$  and 1.644 $\mu\text{m}$   $\text{a}^4\text{F}_9\text{--a}^4\text{D}_7$  [FeII]. Both the [FeII] line and HI Br12 rest wavelengths are indicated by the dotted lines. The spectra are presented in the rest frame after correction for their published  $v_{\text{LSR}}$  values for easier comparison.

can then be used to apply a correction factor to the data. Generally such corrections are small ( $<1\%$ ) but important in obtaining the best possible signal-to-noise ratio from the acquired data.

Wavelength calibration was achieved using the telluric atmospheric absorption features present in all spectra. There are significantly more of these than either arc lines or night sky lines and hence they provide a much better map of the distortion of the wavelength scale and of the variation from object to object. We measured the wavelengths of the absorption features from the much higher spectral resolution atmospheric absorption spectrum published by Hinkle, Wallace & Livingston (1995). Comparison of the different HI Brackett lines showed this procedure gave consistently good results, allowing us to compare the different lines with confidence. Our observations of NGC 7027 indicated our wavelength calibration should be good to within  $\pm 8 \text{ km s}^{-1}$ .

Finally, after objects are ratioed with the standard stars the two beams are combined to give the final flux calibrated spectrum. The final spectra are shown in Figure 1.

### 3 RESULTS

#### 3.1 General Properties

The hydrogen Brackett Br11 and Br12 lines were detected in all objects observed, as is evident in Figure 1 and Br $\gamma$  is also present in all 5 sources we observed at that wavelength as shown in Figure 3. We also detected the  $1.688 \mu\text{m } z^4\text{F}_9\text{--}c^4\text{F}_9$  FeII in all sources, though in M8E it is very weak. Forbidden [FeII] emission was also clearly present in BD+40°4124, M17SW IRS1, MWC 349A and S106 IRS. In S106 IRS the [FeII] emission is extended, with a strong velocity gradient along the full length of the slit. The bulk of the emission for our slit position angle comes from the north-eastern cone of the bipolar nebula (Solf & Carsenty 1982), and is blueshifted with regard to the systemic velocity. For each of these four objects the [FeII] line width was  $50 \text{ km s}^{-1}$  or less. The [FeII] line is a known tracer of fast shocks, such as seen in collimated outflows near young stellar objects, and the line widths observed are perfectly consistent with this explanation. There is also a weak broad feature in both GL 490, and possibly VV Ser, that may be due to [FeII] but is offset to the blue from the systemic velocity (by about  $60 \text{ km s}^{-1}$  and  $10 \text{ km s}^{-1}$  respectively). However the width of the line in these cases, about  $100 \text{ km s}^{-1}$  for VV Ser and  $200 \text{ km s}^{-1}$  for GL 490, suggests a different origin from the other sources unless we are seeing a one-sided jet coming towards us in these sources. These are the also two lowest luminosity sources we observed. We have been unable to identify any possible alternative identification, but it seems probable that the line seen is not [FeII]. With these two exceptions, the forbidden [FeII] emission has a very different line profile from the FeII line, and is always much narrower than any of the other lines observed. In addition, the [FeII] line is seen in NGC7027 whilst the fluorescent FeII is not, as expected for a purely nebular origin for the emission in this source. We can be confident therefore that the [FeII] line has an origin in the extended nebular gas around our sources when present, and FeII line has a different origin. We will not consider the [FeII] line further in this paper since we primarily observed

it to demonstrate that the fluorescent FeII emission was not excited in a similar fashion to the [FeII] emission.

An otherwise previously unidentified line at  $\sim 1.68955 \mu\text{m}$  is clearly visible in GL 490, M8E, MWC 297 and MWC 349A, and possibly in S106 IRS. In S106 IRS the width and double peaked nature of the main FeII line blends with this feature, making the exact identification difficult, but there is excess red emission present that would naturally be explained if this unidentified line was also present here with a similar profile to that of Br12 and FeII. Both FeI and CI lines are identified at  $1.68959 \mu\text{m}$  in the solar spectrum (Ramsauer, Solanki & Biemont 1995). Observations of FeI 8387Å in IRC+10420 (eg. Oudmaijer 1998) show an almost identical line profile to the line shown here in that object (Figure 1). We therefore prefer an identification with FeI for this line. Another unidentified line can be seen near  $1.6385 \mu\text{m}$  in IRC+10420 and possibly M8E, which again might be identified with a blend of two FeI lines (from the atomic data presented in Meléndez and Barbuy 1999). This is certainly consistent with its appearance in only these two objects, but the profile is of poorer signal-to-noise in IRC+10420, which, together with the possible blending, makes it difficult to compare the profile of this line with that seen at  $1.68959 \mu\text{m}$ .

Figure 2 and Figure 3 present the key observational results that we will interpret in the rest of this paper, namely a comparison of the profiles of the FeII, Br12 and Br $\gamma$  lines. The continuum has been subtracted from all the profiles. We note that weak HeI line emission is present in both S106 IRS and MWC 349A, on the blue wing of Br12 and, more obviously, Br $\gamma$ , but we have not attempted to correct for this. We have corrected the observed lines for extinction in order to make a detailed comparison. We adopt the extinction law from Cardelli, Clayton & Mathis (1989) to convert the literature values in Table 1 to  $A_H$  and  $A_K$ , using the standard value of  $R = 3.1$ . The data shown in Figure 2 and Figure 3 have had these corrections applied. Finally we have normalised the plotted data such that the peak intensity of Br12 is given a value of unity, and all other corrected fluxes scaled relative to this.

In order to compare the data with previously published work, and as a crude guide to the properties reflected by the observed line emission, we have also fitted all of the lines with a Gaussian. This was done to determine the systemic velocity as measured by that line,  $v_{LSR}$ , and the approximate full width at half maximum (FWHM). Where double peaked line profiles are present single Gaussian fits were used to measure line centre and FWHM, with the fit restricted to the line wings. This gives reasonably accurate values for  $v_{LSR}$  but the line width is only accurate to approximately 10%, and the quoted error reflects this. The full width at zero intensity (FWZI) is measured from the point where the line is  $3\sigma$  above the noise level, after smoothing the data by a factor of two, for direct comparison with the data presented in Bunn et al. (1995). The results are shown in Table 2.

Finally we note that the objects are split almost evenly between those where the overall general line shape is similar in Br12 and FeII, and those which show significant differences. However, the hydrogen lines are as broad or broader than the FeII line as measured at the half maxima points, and in BD+40°4124, GL 490, M17SW IRS1 and VV Ser the

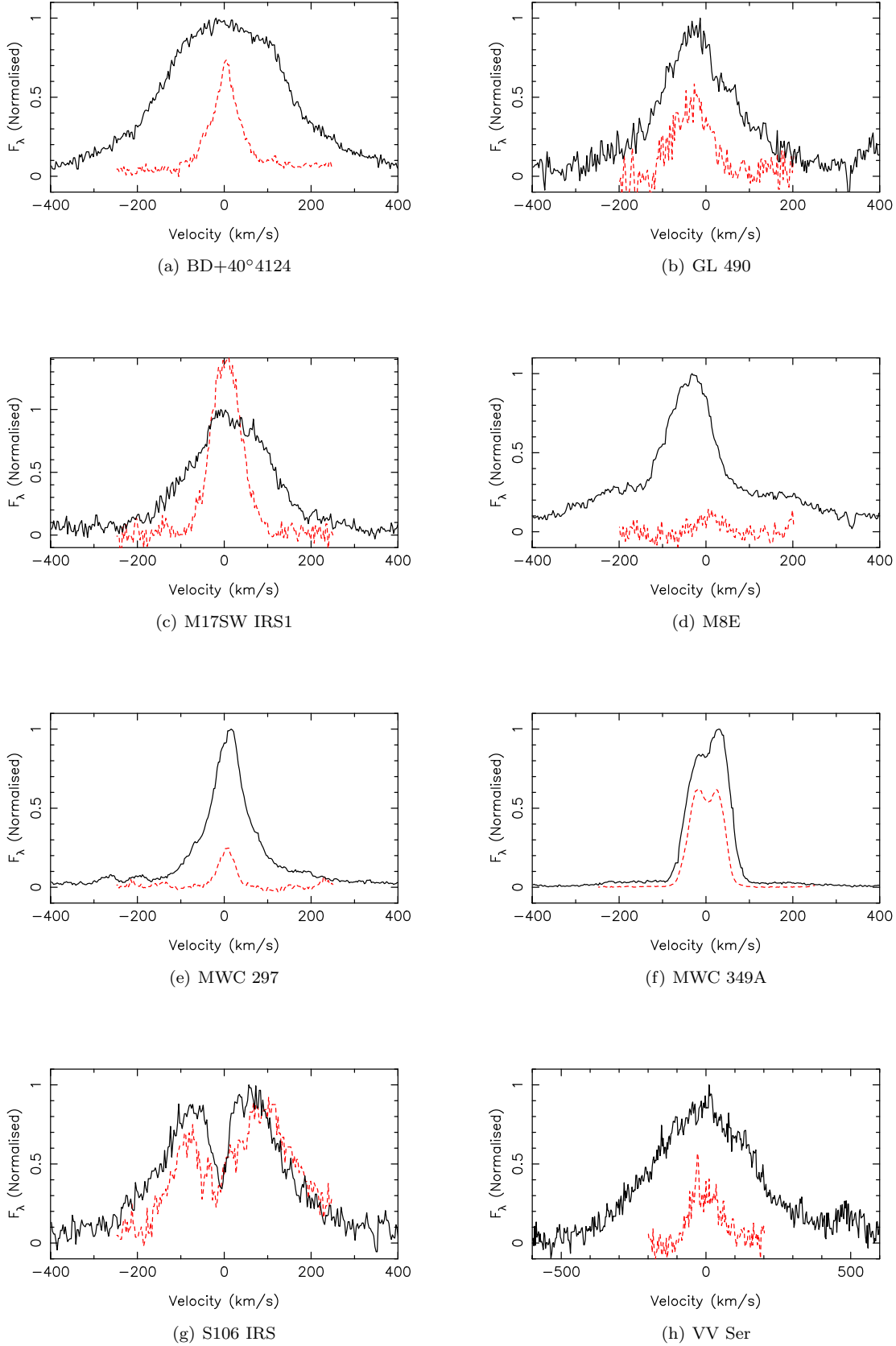


**Figure 2.** Br12 (solid) and FeII (dashed) line profiles after continuum subtraction. The velocity scale for all objects is in their own rest frame, after correction according to the nominal  $v_{LSR}$  values given in Table 1. The spectra are normalised so that the peak flux of Br12 is set equal to 1, and the FeII line is scaled relative to this.

Object	Br12				Br $\gamma$				FeII			
	$v_{LSR}$	FWHM	FWZI	Flux	$v_{LSR}$	FWHM	FWZI	Flux	$v_{LSR}$	FWHM	FWZI	Flux
BD+40°4124	14 $\pm$ 1	320 $\pm$ 30	$\pm$ 510	1.61 $\pm$ 0.05	8 $\pm$ 1	233 $\pm$ 1	−500/ + 530	3.2 $\pm$ 0.1	3 $\pm$ 1	74 $\pm$ 1	$\pm$ 100	0.29 $\pm$ 0.01
GL 490	−24 $\pm$ 1	192 $\pm$ 1	$\pm$ 275	0.4 $\pm$ 0.02					−32 $\pm$ 1	97 $\pm$ 1	$\pm$ 80	0.1 $\pm$ 0.01
M17SW IRS1	14 $\pm$ 1	210 $\pm$ 20	−420/ + 330	0.3 $\pm$ 0.02	8 $\pm$ 1	163 $\pm$ 1	$\pm$ 550	1.3 $\pm$ 0.01	4 $\pm$ 1	80 $\pm$ 1	$\pm$ 80	0.1 $\pm$ 0.01
M8E	−37 $\pm$ 1	116 $\pm$ 3	−600/ + 730	0.9 $\pm$ 0.05					9 $\pm$ 1	71 $\pm$ 2	$\pm$ 55	0.02 $\pm$ 0.01
MWC 297	10 $\pm$ 1	64 $\pm$ 1	−375/ + 400	12.4 $\pm$ 0.01					6 $\pm$ 1	44 $\pm$ 1	$\pm$ 50	1.06 $\pm$ 0.03
MWC 349A	7 $\pm$ 1	83 $\pm$ 8	$\pm$ 330	24.0 $\pm$ 0.1	15 $\pm$ 1	97 $\pm$ 10	−300/ + 400	120 $\pm$ 1	2 $\pm$ 1	68 $\pm$ 7	$\pm$ 100	13.50 $\pm$ 0.05
S106 IRS	−6 $\pm$ 1	280 $\pm$ 30	$\pm$ 420	0.39 $\pm$ 0.02	−1 $\pm$ 1	185 $\pm$ 20	/ + 380	4.54 $\pm$ 0.01	19 $\pm$ 1	235 $\pm$ 20	−200/	0.13 $\pm$ 0.02
VV Ser	−18 $\pm$ 1	380 $\pm$ 2	$\pm$ 420	0.52 $\pm$ 0.1	−3 $\pm$ 1	320 $\pm$ 5	−600/ + 700	2.1 $\pm$ 0.1	−6 $\pm$ 1	110 $\pm$ 10	$\pm$ 80	0.07 $\pm$ 0.01

**Table 2.** Measured observed line parameters: all velocities are quoted in  $\text{km s}^{-1}$ , and all fluxes in units of  $10^{-15} \text{W m}^{-2} \mu\text{m}^{-1}$ . The FWZI missing for the blue wing of Br $\gamma$  and the red wing of the FeII line in S106 IRS are due to strong residual line emission on the wings of the tabulated lines from other species. The errors quoted are the nominal errors on the fit, and do not include any error in the velocity calibration itself.

difference is a factor of 2–3 as is easily seen in Figure 2 and Table 2. The hydrogen lines also have much higher velocities in the line wings as measured at zero intensity, with the possible exception of S106 IRS. In all cases the velocities observed are too large to be explained by gas excited in a standard HII region. There is a rough trend for more inclined objects to have broader Br12 lines, as would be expected when the motions in the disk plane are more along our line of sight (eg Horne and Marsh 1986).

### 3.2 Comparison of the hydrogen line profiles

The comparison of velocity resolved hydrogen line ratios can potentially reveal the origin of the emission. If the gas is optically thin, this ratio will be a constant and will tend towards the case B ratio (eg Storey & Hummer 1995). Bunn et al. (1995) however showed it was possible to define the origin of the emission in the case where the lines are at least partially optically thick. Br11 and Br12 are too close together to provide a useful comparison of line opacity (and as noted above we discount the Br11 lines from analysis given the problems associated with its location near the edge of the observed spectra). We did observe BD+40°4124, M17SW IRS1, MWC 349A, S106 IRS and VV Ser in both Br $\gamma$  and Br12 lines. Figure 3 shows the Br $\gamma$  and Br12 lines for each of these objects, corrected for the inferred extinction as described in Section 3.1, as well as the ratio of these lines. Away from the bright line cores, the main source of noise is actually non-Gaussian read-noise from the array. We have therefore truncated the line ratio plots at the velocity where the noise starts to dominate the ratio, but it is evident from the over-plot of the lines themselves that the ratio remains roughly constant even beyond this. The presence of HeI emission is evident in MWC 349 and S106 IRS, at a systemic velocity of  $\sim -200 \text{km s}^{-1}$  relative to Br $\gamma$ , as a turn-up in the ratio at that point.

The ratio in absorption cross-section between Br $\gamma$  and Br12 is 11.1, whilst that between Br $\alpha$  and Br $\gamma$  is 15.9, and Br $\alpha$  and Pf $\gamma$  is 14.0. The comparison of Br $\gamma$  and Br12 is therefore a valuable test of the line formation mechanism in the same sense as the comparison of Br $\alpha$  and Pf $\gamma$  or Br $\gamma$  in the work of Bunn et al. (1995). For the two objects we have in common with Drew et al. (1993) and Bunn et al. (1995), the line ratios actually show very similar results near the systemic velocity (Figures 3(b) and 3(d)). The earlier data have slightly lower spectral resolution and are also of lower

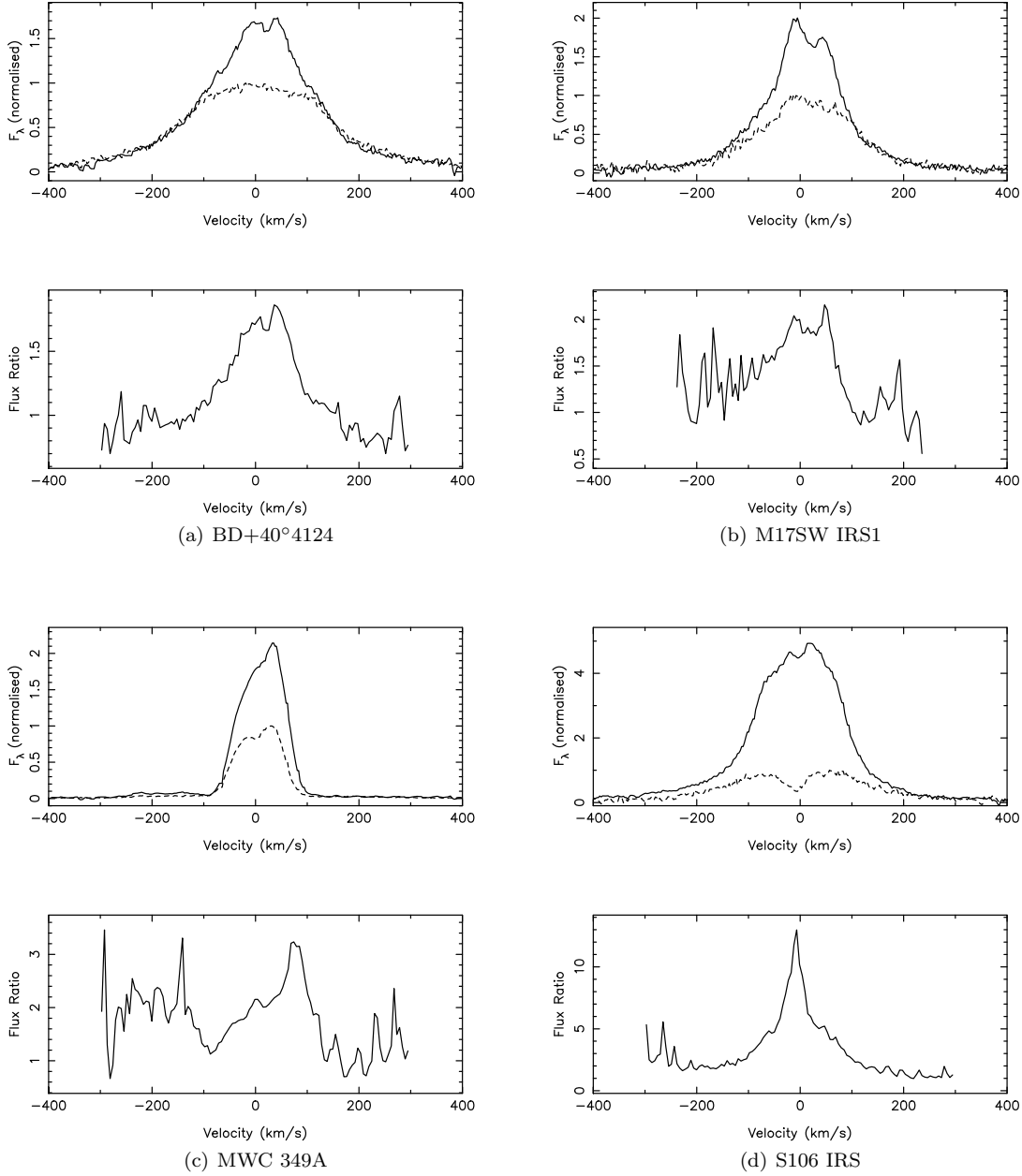
signal-to-noise, which together can explain any differences seen.

The optically thin case B value of the Br $\gamma$ /Br12 ratio is  $\sim 5 \pm 1$  for values of the electron density in the range  $10^4 - 10^9 \text{cm}^{-3}$  and temperature in the range 3000 – 30000K (Storey & Hummer 1995). Simple theory indicates that for completely optically thick lines the ratio of the intensities of the two should scale simply as  $I_1/I_2 = (\lambda_2/\lambda_1)^4 (S_1/S_2)$  in the Rayleigh-Jeans limit, where  $S_1$  is the effective surface area of the emitting region of line 1. If the emitting region of the two lines has the same surface area then the limiting ratio is  $\sim 0.36$  for Br $\gamma$ /Br12. In practice we would expect the lower excitation Br $\gamma$  line to emit from a larger volume, and hence larger surface area, so a value somewhat above this would be expected for gas which is close to optically thick. Figure 3 shows all five objects, with the exception of gas near the systemic velocity in S106 IRS, lies between the case B and optically thick limit, indicating opacity in at least one of the Brackett lines. Overall the trend in the ratios is very similar for four of the objects, namely a largely symmetrical profile that peaks near systemic. The exception is MWC 349, which has a very asymmetrical profile. We therefore defer a full discussion of a suitable model for MWC 349 to Section 3.4.6.

The generic features that any theory for the origin of the hydrogen line emission must be able to explain can be summarised as follows. First, we reiterate that all of our sources show all of the observed hydrogen lines in emission, and the objects show evidence for nearly symmetric very broad line wings (Figures 2 and 3). Secondly, many of the line ratios tend to be closer to the optically thick limit ( $F_{Br\gamma}/F_{Br12} \sim 1$ ) in the line wings than in the core. Last, three of the objects show evidence for weak double peaked or self-absorbed line profiles, in either Br12 or Br $\gamma$  or both. In two of the sources the minimum is significantly offset from the systemic velocity: in BD+40°4124 it lies at  $\sim 21 \text{km s}^{-1}$ , and in M17SW IRS1 at  $\sim 25 \text{km s}^{-1}$ . In S106 IRS however it lies at  $\sim -3 \text{km s}^{-1}$ . This however is within the error on our velocity scale, and hence is also in practice consistent with a small redshift. The first two are suggestive of self-absorption due to infalling material. The latter may still be self-absorption, or an intrinsic double peaked profile centred on the systemic velocity. These three objects are either at intermediate inclination angles or close to edge-on (Table 1).

These characteristics are shared by at least some lower mass pre-main sequence stars as well. Folha & Emerson (2001) present Br $\gamma$  spectra of a large number of T Tauri



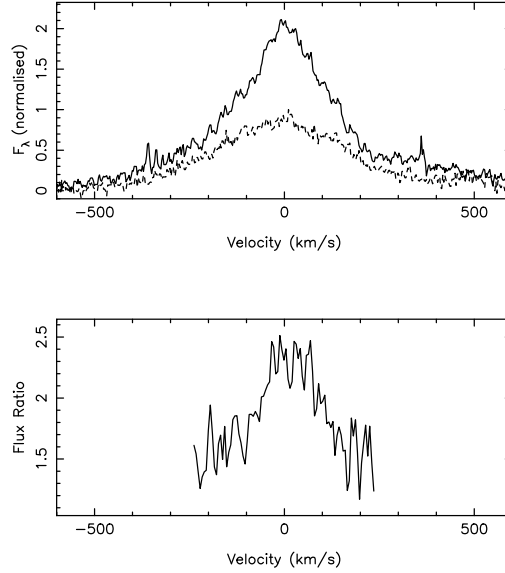


**Figure 3.** Br $\gamma$  and Br12 line profiles after continuum subtraction, and correction for extinction. The Br12 line has been scaled as in Figure 2, and the Br $\gamma$  line scaled relative to this. HeI  $7^3,1G-4^3,1F$  emission is evident in MWC 349A between a velocity of  $\sim -250 \rightarrow -100 \text{ km s}^{-1}$  on the Br $\gamma$  spectrum. The same emission is also present in S106 IRS though only shows because of the asymmetry of the blue and red line wings to Br $\gamma$ . We have not attempted to correct the plotted ratio for this HeI emission. The ratio shown is for the line profiles after the corrections stated above have been applied. The ratio is smoothed by a factor of two relative to the line profiles, and truncated at the point where noise becomes dominant as noted in the text. The velocity scale is in the rest frame of the object as in Figure 2.

stars. Symmetric broad wings and weak Br $\gamma$  line self-absorption are common in the objects they class as type I under the scheme of Reipurth, Pedrosa & Lago (1996: type I objects in the original work refer to objects with symmetrical and unabsorbed H $\alpha$  profiles). These are all objects that show greater evidence of veiling in the continuum, which is usually taken to indicate a high accretion rate. Objects without this veiling show less evidence for strong broad emission lines. It is worth noting that many of the strong T Tauri Br $\gamma$

line emitters still show P-Cygni style wind absorption, but only in the HeI lines that end in the metastable  $2^{1,3}S$  levels (eg for the  $1.083\mu\text{m } 2^3S - 2^3P$  line, Edwards et al 2006). Many Herbig Ae/Be stars also show pronounced P-Cygni profiles for the HeI  $1.083\mu\text{m}$  line (Oudmaijer et al. 2011) as does MWC 297 (Drew et al. 1997), and another object in our sample, S106 IRS, has a P-Cygni profile in the  $2.058\mu\text{m}$  HeI  $2^1S - 2^1P$  line (Drew et al. 1993).

The natural explanation for the HeI profiles is an out-

**Figure 3** – *continued* (e) VV Ser

flowing wind. The terminal wind velocity is then given in the usual fashion by the blueshifted absorption. For both of the objects in the sample under consideration here, S106 IRS (Drew et al. 1993) and MWC 297 (Drew et al. 1997), this gives a probable terminal velocity of  $\sim 200 \text{ km s}^{-1}$ . The wings on the hydrogen lines are still broader than this however (cf Figure 3). In addition the wings have approximately the same full width at zero intensity in Br12 as Br $\gamma$ . As noted by Bunn et al. (1995), if an *accelerating* wind is present the expectation is that the Br $\gamma$ /Br12 line ratio should increase at high velocities: the faster gas lies physically farther out, in less dense gas, and is therefore optically thinner, and therefore the full width at zero intensity should reduce for higher series members. None of our observed ratios match this. We can therefore rule out a standard hot star accelerating wind as the source of the emission. A decelerating (perhaps mass loaded) or constant velocity wind cannot be ruled out however.

The obvious alternative would be a variant on a disc model. However, this would be expected to show double peaked line emission if edge-on and relatively narrow emission without broad wings if face-on for a pure disc model. A combination of wind and disc might appear to solve the problem, but such a geometry effectively masks much of the receding emission in stars that are near face-on and the symmetry of the lines argues against this being the sole mechanism responsible (see Section 3.4.5). An interesting theoretical study with regard to the modelling of T Tauri stars, by Kurosawa, Romanova & Harries (2011), makes many of these same points about the difficulty of fitting profiles to the strong HeI absorption, Br $\gamma$  emission sources. Their model includes potential emission from a stellar wind, a disc wind and magnetospheric accretion. They are able to reproduce the need for blueshifted absorption in HeI, and mostly symmetric emission in the infrared hydrogen lines. However, the lines are too narrow, and at high mass accretion rate the hydrogen lines start to show inverse P-Cygni absorption from

the infalling gas, suggesting some extra component is required to fully explain the broad wings in the hydrogen lines. Notably, the disc wind also must have a large opening angle to avoid significant self absorption even at relatively low accretion rates, and the same is likely to be true for our sources.

This raises the possibility that additional line broadening may be present in the hydrogen lines. Typical densities of the inner regions of an outflowing wind in these sources are naively of order  $\gtrsim 10^{12} \text{ cm}^{-3}$  assuming the mass loss rate is  $\gtrsim 10^{-6} M_{\odot}/\text{yr}$ , the observed wind velocity of  $\sim 200 \text{ km s}^{-1}$ , and typical main sequence OB star radii. The radius may actually be an underestimate since models predict the stars are swollen until they reach a final main sequence configuration (eg Hosokawa & Omukai 2009), consistent with the low stellar wind speeds we see. However, the mass loss rates are also likely to be substantially higher, so the density estimate is relatively unchanged. This density is large enough that Stark broadening can become significant for some lines (cf Muzerolle et al 2001 for the case of T Tauri stars). Repolust et al. (2005) modelled the Stark broadened Brackett line profiles for main sequence OB stars. Although the winds present in main sequence stars are very different, the density is similar to the estimate given above for our simple outflowing wind, and the principle of whether broadening occurs under such circumstances is identical. Figure 3 in Repolust et al. shows that in this density range wings are easily generated by Stark broadening for Br10, with broad wings similar to that seen in our data. Electron scattering can also be apparent with such high densities. With  $T_e \sim 10000 \text{ K}$ , line wings comparable to the thermal velocity width of the electrons of  $550 \text{ km s}^{-1}$  is possible. We know scattering is significant in some Herbig Be stars, including MWC 297 (eg Oudmaijer & Drew 1999). Another key advantage of a broadening mechanism is that it can help to fill in any depression in the line caused by line self-absorption due to shadowing from a disk (eg see the schematic in Malbet et al. 2007 with regard to

MWC 297). Finally, broadening decouples the line ratio at high velocity from the need for an optically thick emission region at that velocity.

In principle we can even tell which broadening mechanism is actually present. A simple comparison of the ratio of the intensity of the line wing to the peak intensity will show stronger wings for higher series transition if Stark broadening is present, since these are the states most affected by perturbations due to neighbouring ions. We would expect the opposite to be true for electron scattering, where essentially it is the population of the excited state that determines the likelihood of scattering. Thus a line like  $H\alpha$  is more likely to have wings enhanced by scattering, and the relatively high Br series lines we are studying are more susceptible to Stark broadening. Stark broadening should also tend, in the high velocity limit, to wings that scale as  $v^{-5/2}$  (Repolust et al. 2005). The core of the line, as shown clearly in the data of Repolust et al., should also be almost flat in a  $\log F_\lambda$  versus  $\log v$  plot. Scattering has been modelled previously in the young stellar object Lk  $H\alpha$  101 by Hamann and Persson (1989), using the prescription of Castor, Smith and van Blerkom (1970). In this model the scattering all occurs in a slab that lies just above the line source (the stellar wind), and is optically thin to Thomson scattering. Laor (2006) describes a model for scattering in the broad line region in active galaxies, with a similar requirement on the opacity but an isotropic illumination of the electrons, rather than a one sided illumination. The resultant functional forms for the scattered flux are different, but both give profiles that are roughly exponential for likely values of the two key scattering parameters (opacity and electron velocity). In principle, the Castor et al. model can be used to measure these scattering parameters, and hence also quantities such as density at the base of the wind. In practice, this has not proved possible as we shall discuss in our analysis of the best fit to the line profiles in Section 3.4, and in Section 4.

Finally, as noted by Drew et al. (1993), an optically thin nebular component may be required in some cases in addition, of which S106 IRS is a clear example given it powers an extended bipolar HII region (all three Brackett lines presented are visible across an extended region on the long slit spectrum, with lines of width  $\sim 30\text{kms}^{-1}$ ). In that instance the line ratio at systemic velocity is actually above the case B value. This most likely indicates that the optically thin nebular gas actually has lower extinction than S106 IRS itself (ie we have over-corrected for the extinction in this component), which is consistent with the fact the nebula is visible in the optical and the star itself is extremely faint.

Overall therefore, broadening gives a natural explanation for the wings in all our sources. If we accept that factor, then a decelerating, constant wind or large angle disc wind are viable explanations for the core of the lines. This is probably a natural explanation for all massive and intermediate mass young stellar objects since none of our objects are selected to be in any way “special”.

### 3.3 Modelling of the FeII line with a disc

The fluorescent FeII emission is a clear tracer of emission from a disk in classical Be stars (Carciofi & Bjorkman 2006). Detailed models have been derived for observations of the optical FeII lines in Be stars (eg Arias et al 2007), show-

ing that even quite complex line profiles can be explained in terms of emission from a relatively narrow ring. It therefore seems natural to consider whether a disc model can explain these relatively younger objects. Currently, the  $1.688\mu\text{m}$  FeII line is not yet included in any radiative transfer model. Nor do we understand its source function well enough, given its potential origin as a laser (Johansson & Letokhov 2007), to reliably model even in the fashion of Arias et al. We therefore rule out detailed calculations at this point, and leave that to future work. Instead, we adopt a “proof of concept approach” and attempt to fit the observed line profiles with a simple accretion disc model but without a detailed source function for the line emission, or attempting to enforce a correct temperature structure for the emission zone. Specifically, we use the constraints given by other observations to fix the mass of the star and the inclination (as quoted in Table 1), and then test how well a disc can fit the observed line profile.

The model in question consists of a Keplerian disc within which the line flux per unit area is proportional to the local surface density. The structure of the rotating disc is given by the standard  $\alpha$ -disc model – as described by, eg, Pringle (1981). The accretion rate and value of  $\alpha$  are not fitted in this process, since the model is being fitted to a normalised line profile, and thus the actual surface density is unimportant. Furthermore, the variation of surface density with radius is insensitive to both  $\alpha$  and the accretion rate. As a result, the only free parameters are the intrinsic line width and the outer radius of the emitting area. The latter is poorly constrained for most of the objects however since they exhibit single peaked emission. In that instance the outer radius is a lower limit set by the model line width, since we clearly cannot constrain this parameter strongly in the case of a near face-on inclination.

Turbulent line broadening is added to the disc model in order to achieve the final fits. This is represented by a Gaussian, and the width is given in Table 3. No other line broadening mechanism is considered as we do not expect any to occur – even thermal broadening is likely to be insignificant for iron. Indeed, as noted by Johansson and Letokhov (2007), the conditions under which this FeII line is emitted are likely to lead to mild lasing, which actually narrows the natural line profile. We also do not expect the opacity in this transition to be significant.

The model is used to determine the line profiles for a given set of input parameters. The model profiles are then smoothed to the instrumental resolution, before being compared to the observed profiles. To find the best fitting profiles, the outer radius and line width are allowed to vary between  $1\text{--}100\text{AU}$  and  $1\text{--}75\text{kms}^{-1}$  respectively and the Powell method (as implemented in IDL) is used to minimize the residual of the fit. We present a comparison of the best fitting model profiles and the data in Figure 4. A detailed case-by-case discussion of the best-fitting parameters is deferred to the next section, but it is clear that, in general, the observed FeII  $1.688\mu\text{m}$  line profiles can be modelled by emission from circumstellar discs of an appropriate size. The major exception to this is S106 IRS, which we discuss in detail in Section 3.4.7. Figure 2 shows that GL 490, MWC 297 and MWC 349A also appear similar in FeII and Br12 if we ignore the broad Br12 line wings. A disc model can also partly explain the Br12 emission in all of these sources as

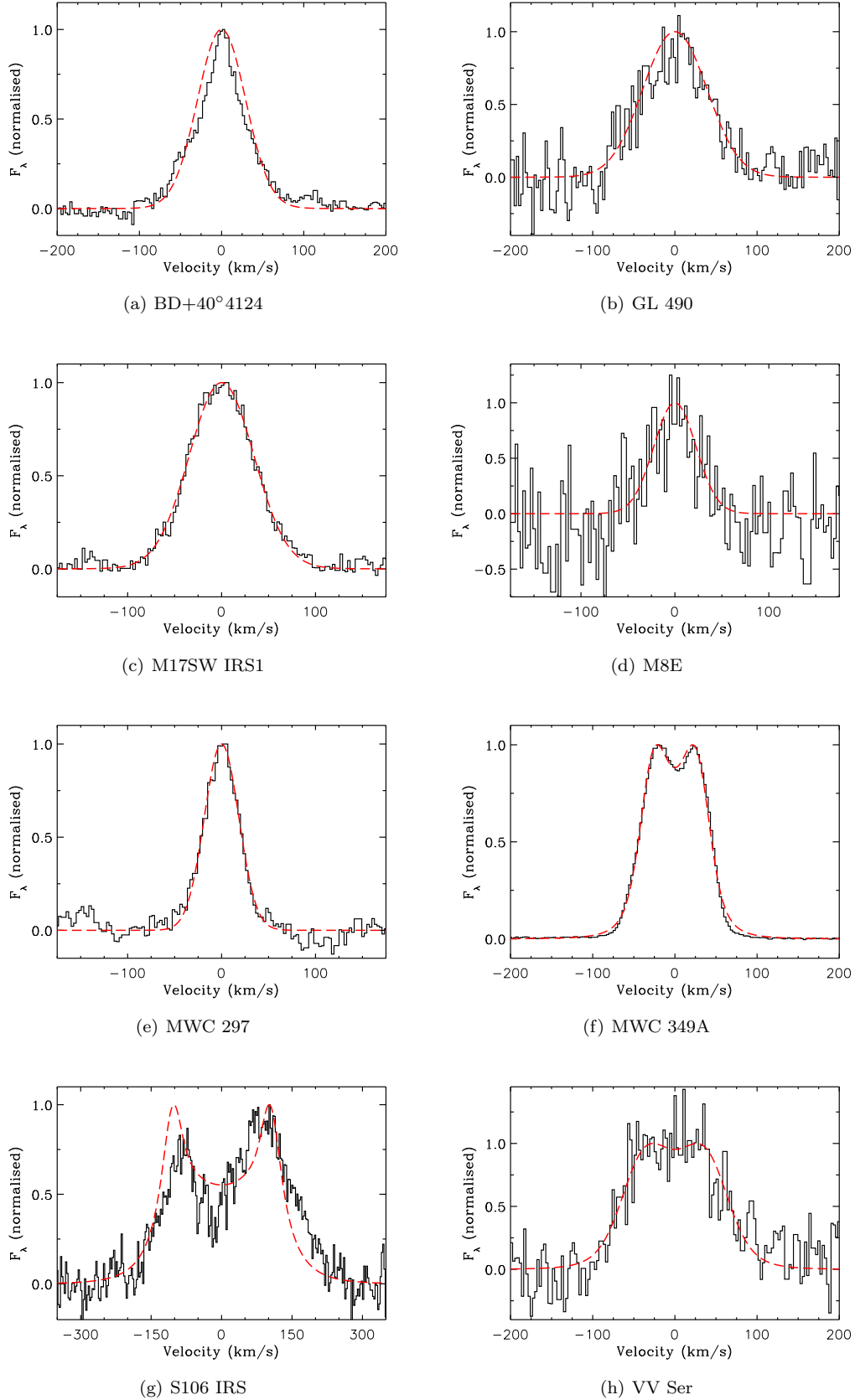


**Figure 4.** FeII emission line profiles of each object and the associated best-fitting disc model profiles (dashed line). In VV Ser the “spike” evident in Figure 2(h) has been clipped to allow a better disc fit to the underlying line profile.

Object	$M_{\star}$ ( $M_{\odot}$ )	$R_{\star}$ ( $R_{\odot}$ )	$i$ ( $^{\circ}$ )	$R_{\text{out}}$ (AU)	Line-width ( $\text{km s}^{-1}$ )	$\chi^2$
BD+40 $^{\circ}$ 4124	6.1	3.56	45	21.6	60.8	4.1
GL 490	8.6	4.28	30	5.2	75.0	0.7
M8E	13.5	5.46	20	15.6	44.6	0.6
M17SW IRS1	15.0	5.80	15	3.7	70.0	0.7
M17SW IRS1			67	67.5	68.8	0.7
MWC 297	10.0	6.12	15	10.5	36.5	0.5
MWC 349A	26.0	8.54	85	31.0	26.4	41
S106 IRS	21.7	7.51	80	1.8	26.8	1.0
VV Ser	3.8	2.81	85	2.0	50.1	0.8

**Table 3.** Parameters of the best fitting models. The stellar radii and masses are taken from the compilation of Harmanec (1988). For M17SW IRS1 we show two fits to the data, one reflecting the inclination inferred by Follert et al. (2010), the other for a more face-on orientation. The fit shown in Figure 4(c) is the former, but there is essentially little difference between the two. The other inclinations are adopted from Table 1

discussed below, consistent with the results from fitting the iron line. A disc model does not fit the HI lines from the other sources well at all.

### 3.4 Comments on individual objects

#### 3.4.1 BD+40 $^{\circ}$ 4124

The H $\alpha$  line in this source shows an asymmetric double peak (Vink et al. 2002), closer to line self-absorption than to evidence for a rotating disk. The velocity separation between the peaks is  $\sim 120 \text{ km s}^{-1}$ , compared to only about  $\sim 40 \text{ km s}^{-1}$  as seen in our Br $\gamma$  spectrum. This is also consistent with the self-absorption picture since we would expect H $\alpha$  to be more optically thick at velocities near, and to the blue of, systemic compared to Br12 if a dense wind is present (as is evidenced by Figure 3(a)). Eisner et al. (2003) find an inner radius of 0.73au from modelling their continuum interferometric data with a flat dusty disc. Any disc within this radius must be dust-free. Vink et al. (2002) find that their H $\alpha$  polarisation data can be explained by a straightforward line depolarisation effect, where the continuum light is scattered by a small scale disc, whereas the emission line itself arises on scales larger than the disc, likely in a wind. The small scale disc could be the extension of the dusty disc detected by Eisner et al. down to the star. The line wing/peak ratio is roughly the same for Br $\gamma$  and H $\alpha$ , but larger for Br12 (cf Figure 3(a)), suggestive of Stark broadening. The line wings can be fitted equally well by both a power-law, with exponent  $\sim -2.0 \pm 0.1$ , and an exponential (Figure 5). We also explicitly fitted the Castor et al (1970) model. A formally good fit is achieved, but the key parameters in this case, the width of the line core, the electron temperature (width) and opacity, are highly degenerate. Effectively there is little difference between a very broad intrinsic line and a highly scattered one. The wing-peak ratio for the Br12 and Br $\gamma$  data, and the closeness of the power-law exponent to the canonical  $-2.5$ , both suggest that Stark broadening is present however. The FeII emission in this object is not fitted perfectly by a disc model, but the profile is clearly very different from the Brackett lines. In this instance it is plausible that the hydrogen lines arise in a large scale wind, whereas the FeII is mostly tracing the inner disk.

#### 3.4.2 GL 490

Schreyer et al. (2006) detect a relatively large-scale ( $\sim 1500 \text{ au}$ ) molecular disc in approximate Keplerian rotation from which they derive an inclination of  $\sim 30^{\circ}$ . The position angle for this disc is the same as that found at 2cm by Campbell, Persson & McGregor (1986), and both lie orthogonal to the direction of the observed large scale molecular outflow observed by Mitchell et al. (1995), similar to other equatorial wind systems (eg Hoare 2006). Oudmaijer, Drew & Vink (2005) also inferred the presence of a small scale disc from near infrared spectropolarimetry. Oudmaijer et al. did however require the initial line emitting material to lie internal to the scattering disc, and that the disc did not extend down to the stellar surface.

Our Br12 profile looks very similar to the Br $\gamma$  profile in Bunn et al. (1995). Bunn et al. also infer a relatively flat Br $\alpha$ /Br $\gamma$  ratio in GL 490 out to velocities  $\sim \pm 100 \text{ km s}^{-1}$ , before an upturn is seen. However, the evidence for a turn-up in these earlier CGS4 data may be compromised by poorer continuum subtraction, since the data were taken with a smaller array and at lower spectral resolution, spatial resolution and free spectral range. Comparison of our Br12 profile with the Br $\gamma$  and Br $\alpha$  profiles in Bunn et al. suggests that the broad line wings are relatively stronger in Br12 which slightly favours Stark broadening. There is a good fit to the Castor et al model for Br 12 as well, and in this instance the parameters are well defined with  $\tau \sim 0.3 \pm 0.05$  and  $T_e \sim 340 \pm 30 \text{ K}$ . The very low value of the electron temperature implied by the fit is a concern, but we do not have sufficient signal-to-noise to determine if the wings extend further in velocity. The line wings do not follow the expected power law for Stark broadening either, having an exponent of only  $\sim -1.2 \pm 0.2$ . In this instance, the relatively poor signal-to-noise prevents a truly firm conclusion.

The Brackett lines differ from the FeII line largely in a strong red asymmetry, and stronger evidence for broad line wings in the hydrogen lines. The FeII emission can be successfully fitted with a Keplerian disc. The inferred lower limit to the outer radius is much smaller than the size of the structure seen in the radio map which is several hundred AU across. Given the similarity of the line core in this object between Br12 and FeII it is possible that a disc may be a suitable explanation for the hydrogen line emission as well, especially given the orientation of the radio emission. There is no self-absorption in any of the lines observed either here

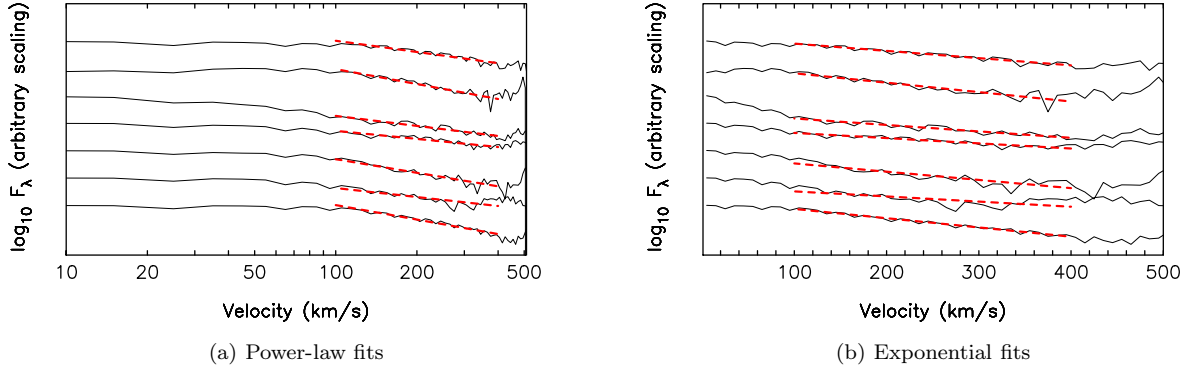


**Figure 5.** Fits to the Br12 line for either a power law or an exponential. The fits are shown as the thick dashed (red) line. The data have been binned into  $10\text{km s}^{-1}$  bins, and folded around the systemic velocity. The fits are made only to the region between  $100$  and  $400\text{km s}^{-1}$ . The objects shown in each plot are (from top down): VV Ser, S106 IRS, MWC 297, M8E, M17SW IRS, GL 490 and BD+40°4124.

or in Bunn et al. so there is no requirement for a strict wind component to be present.

#### 3.4.3 M17SW IRS1

M17SW IRS1 is a young binary star located just beyond the edge of the M17 HII region and is also known as the Kleinmann-Wright object (Kleinmann & Wright 1973). Estimates of its luminosity range from about  $5000 L_{\odot}$  (Chini et al. 2004) to  $50000 L_{\odot}$  (Follert et al. 2010). The latter is more consistent with the presence of HeI  $2.058\mu\text{m}$  emission as reported by both Porter et al. (1998) and Hanson et al. (1997).

The dereddened flux ratio is very similar to that presented by Bunn, Drew & Hoare, and as noted by them is rather similar to that for BD+40°4124. Br $\gamma$  does show weak red asymmetric self-absorption which might suggest the presence of infalling ionised gas.

The Br12 and FeII emission have very different profiles, again in a similar fashion to BD+40°4124. The FeII data can be explained by a disc, at both a near edge-on inclination as measured by Follert et al. (2010), as well as nearer to face-on (cf Table 3). However, an edge-on disc requires a very large spread in the FeII emission region, almost out to the full extent of the mid infrared emission region seen by Follert et al. Without further information however we cannot rule out either possibility. The degeneracy between inclination and outer radius of disc is of course a well known problem in this situation, but M17SW IRS1 is the only source in which the result of fixing the inclination at the value given in Table 1 leads to results that are then difficult to interpret in light of other data. The most likely model for this source is the same as discussed for BD+40°4124, namely a disc giving rise to the FeII emission and a wind the Brackett line emission. The wings on Br12 are relatively weak in this source, but the power law profile of the wing is  $\sim -1.8 \pm 0.2$ , suggesting that Stark broadening may be present. A formally good fit to the Castor et al model can be achieved but the values of both opacity and electron temperature are again highly degenerate with the core line width, and no meaningful physical parameters can be obtained.

#### 3.4.4 M8E

The Br12 line in M8E is best described as a relatively narrow Gaussian superposed on a much broader “pedestal”. This is qualitatively different from the Br $\alpha$  and Br $\gamma$  profiles in Bunn, Drew & Hoare. The line core is similar to Br $\gamma$ , but the higher velocity line wings are less evident. Br $\alpha$  has broad wings but the profiles are not a match. It is possible the greater wavelength coverage of the data presented here may partially explain this difference. It cannot be explained easily with simple line broadening mechanisms outlined in Section 3.2 since there is no simple trend with quantum number  $n$ . An exponential fit is a better match to the broad wings than a power-law, and the latter also has a very low exponent of  $-1.1 \pm 0.1$ . Neither matches at the highest velocities however. The Castor et al model is formally a very poor fit.

One other notable aspect of our data is that the line centre velocity of the Brackett lines are significantly offset with respect to systemic. As shown by Table 2, these lines have  $v_{LSR} \sim -37\text{km s}^{-1}$ , whereas the FeII line has  $v_{LSR} \sim 9\text{km s}^{-1}$ , which is in agreement with the measured molecular gas value, and the Br $\alpha$  and Br $\gamma$  data of Bunn et al. (1995). The fact that both Br11 and Br12 lines agree in velocity rules out a simple wavelength error in part of the data since they are observed in different echelle settings. Bunn et al. infer a relatively flat Br $\alpha$ /Br $\gamma$  optically thick ratio in M8E out to velocities  $\sim \pm 100\text{km s}^{-1}$ , with only weak, if any, evidence of a turn-up at higher velocity.

The FeII line can be modelled by a disc, but the relatively weak line emission is noisy and hence does not particularly constrain other models. Linz et al. (2009) can only set an upper limit on the size of the disc in the mid-infrared of  $\sim 100\text{AU}$ , which is consistent with our FeII disc model. The similarity of the core of the Br12 line and the FeII line, if we ignore the velocity offset mentioned above, suggests both have a common origin. Overall though the difference in velocity, the unusual “pedestal” on Br12 and the fact that the line widths do not simply scale with  $n$  all make it difficult to ascribe an origin to the emission.

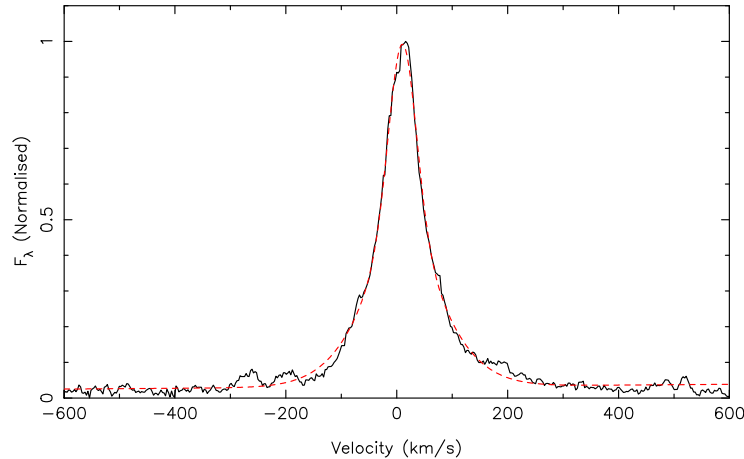


**Figure 6.** The best fitting Castor et al. (1970) model to MWC297.

#### 3.4.5 MWC 297

The inclination of this source is the subject of debate. Drew et al. (1997) find a near edge-on inclination is necessary to explain the observed optical absorption line data, since otherwise the star is near break-up velocity. By contrast all of the interferometry data is best modelled by a near face-on orientation instead. An edge-on model is also more likely to lead to double-peaked line profiles if an ionised disc is a contributor. For consistency with the other objects studied here, where we have adopted inclinations from interferometric data, we do the same here.

The  $\text{Br}\alpha/\text{Br}\gamma$  ratio presented in Murdoch & Drew (1994) is similar to the  $\text{Br}\gamma/\text{Br}12$  ratio of BD+40°4124 or M17SW IRS1 shown in Figure 3. The line widths we measure are similar to the  $\text{Br}\alpha$  width as reported in Drew et al. (1997). The FWZI of  $\text{Br}12$  is closer to that seen in  $\text{H}\alpha$ , though, as is clear from Drew et al., the latter has a much larger FWHM. The  $\text{FeII}$  profile does not show the same broad wings. Most published spectra of MWC 297 show symmetric Brackett line profiles. The exception is Malbet et al. (2007), where a clear blue-shifted asymmetric self-absorption is present in  $\text{Br}\gamma$ . The higher spectral resolution data presented by Murdoch & Drew (1994) or Weigelt et al. (2011) do not show this, which suggests variability is present. There is a clear P-Cygni effect seen in the  $1.083\mu\text{m } 2^3\text{S}-2^3\text{P HeI}$  line (Drew et al. 1997), suggesting a wind is present, which for a relatively face-on orientation must either be a polar wind or a disc-wind with a large opening angle.

Drew et al. present a 5GHz radio map showing resolved radio emission from this source on the scale of  $\sim 50\text{AU}$ , and both the Malbet et al. and Weigelt et al. interferometry also show the core  $\text{Br}\gamma$  emission is more extended than the K-band continuum light. The higher spectral resolution data of Weigelt et al. show the visibility is essentially the same as the continuum beyond about  $60\text{kms}^{-1}$  from the line centre. The  $\text{Br}12$  wings is better fitted by an exponential in this case. Notably this is the only object in which the line core clearly has greater flux than a simple extrapolation of the exponential fit might suggest (Figure 5(b)), as we would ex-

pect if the exponential wings were light scattered from that core. A power-law fit by comparison again has a rather low exponent of  $-1.3 \pm 0.1$ , and the flat inner line core from Stark broadening seen in the Repolust et al. data, and objects such as BD+40°4124, is absent here. Comparison of the strength of the line wings to peak intensity in the hydrogen recombination lines in the data presented here and in Drew et al. (1997) indicates that the wings grow stronger for the lower  $n$  transitions in a fairly uniform way. This is strongly suggestive of electron scattering. The fact that the wings and continuum appear to have the same visibility in the Weigelt et al. data suggests this scattering occurs on small scales.

We consider the scattering model in more detail for MWC 297 since this source shows the best evidence that it is present. The best fit of the Castor et al model has a reduced  $\chi^2 = 2$ , indicative of the fact that the line is slightly asymmetric. We show the fit for this source in Figure 6. In this case the opacity to Thomson scattering is greater than unity, so the conditions on the actual model are not met. The implied electron temperature is also very low ( $T_e \sim 170 \pm 10\text{K}$ ) and not physically meaningful. The match of the Castor et al profile in a case where the intrinsic line core itself is very narrow does argue for scattering being the dominant mechanism, but that this model itself is insufficient to accurately estimate key physical parameters related to the scattering.

If we accept a mostly face-on inclination for this source then our  $\text{FeII}$  profile can be fitted well by a disc model, with an outer radius that is well within the extent of the ionised gas as seen in the radio map. Acke et al. (2008) struggled to fit their combined near and mid-infrared interferometry with a pure accretion disc model, suggesting that more than one component was present. Malbet et al. suggest a combination of disc and a weak outflowing wind can explain their near infrared interferometry and the observed P-Cygni profile they find in  $\text{Br}\gamma$ , but they struggle to find a good fit to the red wing of the  $\text{Br}\gamma$  line because their model predicts disc shadowing should be present where none is seen. The same is true of the models applied to the high spec-

tral resolution observations of Weigelt et al. (2011) as well (which otherwise reach a very similar conclusion to Malbet et al). However the relatively clear evidence for significant scattering in the line wings largely reduces this problem. In a face-on orientation, the lack of a clear line effect in the spectropolarimetry of Oudmaijer & Drew (1999) is not significant, since an asymmetry in the source structure as seen on the sky is required to give rise to such a signature, and this is naturally not present. A counter argument to this is that Weigelt et al. find evidence from the differential phase for a rotational signature in Br $\gamma$ , which of course we would not see in an almost completely face-on situation. An intermediate inclination, as suggested by Acke et al. (2008) as a compromise, may help to reconcile all of these pieces of evidence.

### 3.4.6 MWC 349A

MWC 349A clearly shows different line profiles and ratios to our other sources. The precise evolutionary status of MWC 349A is not known (see, eg, Hofmann et al. 2002 for a discussion), nor is an exact spectral type known. The main argument against it being young is that it lacks significant far-infrared thermal dust emission, with the dust emission peaking in the mid-infrared instead. The strong emission line spectrum and bolometric luminosity are also consistent with an identification as an evolved B[e] supergiant, though it also lies at the upper end of properties of known Herbig Be stars. The luminosity is  $6 \times 10^4 L_{\odot}$  (adapted from Cohen et al. 1985 using the distance from Meyer et al. 2002). This is consistent with the presence of HeI lines in the spectrum (eg Hamann & Simon 1986). MWC 349A shows strong hydrogen maser recombination lines in the mm and radio regime (eg Weintraub et al. 2008), consistent with the edge-on inclination found from interferometry.

FeII emission from similar energy levels to the  $1.688\mu\text{m}$  line also show double peaked profiles (eg the  $2.089\mu\text{m}$  FeII line in Hamann & Simon 1986, the optical lines in Hamann & Simon 1988). These lines have been interpreted as having an origin in a disc (Hamann & Simon 1988). Higher excitation FeII lines appear more like the Br $\gamma$  profile we see here, with a distinct line asymmetry (Hamann & Simon 1988). MWC 349A is the object where our data have the highest signal-to-noise, and therefore small departures from a Keplerian disc are easier to identify. This is clear in our FeII disc fit, which formally is very poor. However, this is mostly due to a weak blue-red asymmetry in the observed data, which cannot be modelled within the context of our very simple prescription. Kraus et al. (2000) also had some difficulty in fitting the  $v=2-0$  CO bandhead with a Keplerian disc profile. A disc is clearly present in this source, however, given the maser emission. It may simply be that the disc is not completely Keplerian as also suggested by the maser observations of Weintraub et al. (2008). Danchi et al. (2001) derived an outer radius of about 50AU from near-infrared interferometry, consistent with what we find from modelling the FeII data, and the origin of the mm/sub-mm masers (Thum et al. 1994), though all are rather larger discs than the best fit that Kraus et al. find for their disc model.

The HI Br $\gamma$  profile also appears very similar to that shown in Hamann and Simon (1986), and shows what is likely to be weak blue self-absorption or a very asymmetric

disk. The broad wings can again be ascribed to electron scattering (Meyer et al. 2002), in agreement with the spectropolarimetry of Oudmaijer et al. (2005). The hydrogen lines have generally been interpreted as the combination of emission from a slow stellar wind and a rotating disc (eg Hamann & Simon, 1986, 1988). This wind must be on larger scales than the disc modelled by Danchi et al., since otherwise the velocities would be anomalously low. Another possibility is a disc-wind since the low expansion velocity evident in the hydrogen lines naturally arises in a model where the wind is launched from the disc at some distance from the star (eg Gordon 2003, Hollenbach et al 1994, Sim et al. 2005).

The Br $\gamma$ /Br12 line ratio plot shows a distinctive pattern different from any of either our sources or those presented in Bunn et al. It is however consistent with self-absorption in the lines due to an outflowing wind in the sense that the opacity increases uniformly towards the blue. We also considered the ratio after the individual line profiles had been cross-correlated, in order to compensate for any residual velocity calibration errors that might be present, which could have an effect here given the steepness of the profile. The result shows a slightly flatter line ratio, but still with a distinct slope in the same sense as shown here. Kraus et al. found that the high series Pfund lines were singly peaked with widths  $\sim 50\text{kms}^{-1}$ . This suggests these lines arise in optically thin gas far from the star in the disc-wind, or in the nebula. However such a large scale optically thin Pfund component should be reflected in both the Balmer and Brackett lines as well, and is not. The mid infrared interferometry presented by Quirrenbach, Albrecht & Tubbs (2006) also shows the high excitation mid infrared hydrogen lines are less extended than the dust continuum emission. Instead the Pfund and higher series lines must, on energetic grounds, arise near the central source, and the single peaked nature implies optically thin, approximately spherical, wind emission. It is probable therefore that the infrared recombination lines largely arise from a combination of disc-wind and spherical wind.

### 3.4.7 S106 IRS

S106 IRS is the exciting star of the Sh 2-106 HII region (see, eg, Saito et al. 2009). The HII region is best modelled as a bipolar flow which is almost oriented in the plane of the sky (eg Solf & Carsenty 1982). S106 IRS has a variety of reported extinction values in the literature. The value given in Table 1 is from a fit to the silicate absorption spectrum as measured by ISO in a large beam (van den Ancker et al. 2000) which will be dominated by the emission from S106 IRS. The fits to the CO bandhead by Chandler et al. (1995) shows that a disc of radius 1–2AU is likely to be present.

The Br $\gamma$  and FeII lines in S106 IRS are remarkably similar (Figure 2(g)), though Br $\gamma$  has a larger FWZI than the FeII line. Perhaps the greatest surprise is that despite the near edge-on nature of this source, a disc model is a very poor fit (Figure 4). We observed the FeII line in S106 IRS at two epochs separated by 378 days. The data shown in Figure 2(g) are the average of these observations. There was no evidence that the HI Br11 line varied between these observations but there is some tentative evidence of a change in the FeII line. This is shown in Figure 7 where we plot the data from the two epochs, after slight smoothing to improve



the signal-to-noise. There is a clear dip in the data at the velocity of maximum absorption for the second epoch. We can understand both the line profile and the variability if the FeII line in this case does arise in a clumpy (hence variable) wind. The remaining differences in the line profile between the Br12 and FeII line then are due largely to the differing opacities in the two lines. We already know that S106 IRS shows strong P-Cygni absorption in the HeI  $2^1S-2^1P$  transition at  $2.058\mu\text{m}$  (Drew et al. 1993), indicative of a stellar wind with a high mass loss rate (see also Felli et al. 1984).

The Br $\gamma$ /Br12 ratio plot for this source is similar to the Br $\alpha$ /Br $\gamma$  ratio presented in Drew et al. (1993) but with better signal-to-noise at high velocity. Drew et al. found an upturn at  $v_{LSR} \sim -200\text{kms}^{-1}$  in their Br $\alpha$ /Br $\gamma$  ratio, which they interpret as evidence that Br $\gamma$  is becoming optically thin. However we see no such evidence. Drew et al. tried to deblend the prominent  $5^{1,3}G-4^{1,2}D$  HeI line from Br $\alpha$  at around this wavelength, whereas we have not done the same for the  $2.16475\mu\text{m}$   $7^{3,1}G-4^{3,1}F$  HeI lines which may explain the difference, though it should in theory enhance the upturn in our data and suppress it in theirs. We therefore accept our line ratio as indicative for the source as a whole. A broadening mechanism is therefore required to explain the line wings as in other sources. The Br12 wings have a power law profile with exponent  $-2.0 \pm 0.2$ , similar to the case of BD+40°4124. An exponential or the Castor et al model give a slightly poorer fit. Since our Castor et al model does not match the central absorption we do not consider the fitting parameters further for this source. The enhanced wings seen in the Brackett lines appear more prominently in Br12 than Br $\alpha$  however, more suggestive of Stark broadening.

An almost unresolved nebular core further complicates the picture for our Br $\gamma$ /Br12 ratio. The nebular line arises from a much larger volume than the rest of the emission, and should have a lower extinction correction applied since the HII region is optically visible. This explains why the ratio plotted in Figure 3(d) exceeds the nominal case B value.

Overall most of the lines in this source can be explained by a dense wind (as in Drew et al. 2003) which must be primarily along the equatorial direction to avoid veiling the nebula from the star. In this instance, the FeII emission may also arise from the disc-wind, given the asymmetric wind-like profile it has.

#### 3.4.8 VV Ser

Blake & Boogert (2004) observed the M band fundamental CO transition in this source. Their results show a clear double peaked profile which they model as a disc with  $i = 85^\circ$ , consistent with the interferometry of Eisner et al. (2003). Notably the blue peak of their CO profile is enhanced with a narrow emission component in the same fashion as our FeII profile. This is suggestive of a localised spot of enhanced emission, which must have an origin in a source with constant velocity (ie not the disc), since our data and the Blake & Boogert data are separated by 2–3 years. We do not quite resolve the blue and red peak in this source despite the almost edge-on nature. The disc model fits well despite this if we ignore the extra “spike”. Notably, Eisner et al. (2003) suggest that a disc of similarly small size is present in their interferometry, though they favour one with a puffed up inner geometry. Pontopiddan, Blake & Smette (2011) model

the CO as arising at 3.5au, outside the emission region for the K-band continuum. VV Ser is observed to have a disk shadow, consistent with this modelling (see discussion in Pontopiddan et al. 2011).

The H $\alpha$  profile is asymmetric double peaked (Reipurth, Pedrosa & Lago, 1996) with a velocity separation of  $250\text{kms}^{-1}$  between the red and blue peaks, again suggestive of a weak P-Cygni profile. Our data lack such obvious P-Cygni effects, but the ratio shown in Figure 3.1 is otherwise similar to most of the other objects. An exponential fit to the line wings is marginally preferred. A power-law fit gives an exponent that is again rather shallow at  $-1.5 \pm 0.1$ . The line wings are stronger relative to the peak in the lower series lines for VV Ser (eg Figure 3(e)), which is suggestive of a scattering origin as well. The Castor et al model gives a formally good fit but the opacity and electron temperature are effectively undefined in the result as was the case for other sources due to degeneracy in the best fitting model. A larger wavelength coverage would perhaps have helped identify the source of the broad line wings in this source. A wind origin for the remaining hydrogen emission seems likely given the very different Br12 and FeII profiles, with the latter almost certainly coming from a disc (Figure 2(h)).

## 4 CONCLUSIONS

Our results show clearly that a wide variety of physical environments can be traced using near infrared spectral lines. It is clear that the combination of HI, FeII and, where available, HeI lines can help to disentangle the otherwise complex line profiles observed. Hydrogen line ratios are particularly powerful in showing the need for a line broadening mechanism in all objects except MWC 349. Specifically, data with sufficient spectral resolution and wavelength coverage allowed us to identify a likely origin in Stark broadening in the wings of hydrogen lines in BD+40°4124, M17SW IRS and S106 IRS, and electron scattered wings in MWC 297, and probably VV Ser. Better signal-to-noise, as available with larger telescopes, and an even larger free spectral range would have allowed us to be more conclusive about the origin of the wings in both GL490 and M8E as well.

One important consequence of the presence of strong line broadening mechanisms in the high series infrared hydrogen lines is that, on their own, they are poor tracers of a wind or a disc. A better tracer of a wind are undoubtedly the HeI lines from metastable levels, although, unfortunately, not every young stellar object shows this emission. The hydrogen lines do however provide a means to test for the presence of very dense circumstellar material (through broadening).

We also attempted to utilise the model of Castor et al. (1970) to estimate physical scattering parameters, assuming that was the dominant mechanism. The fits were either highly degenerate in the parameters where the core line width is close to matching that required for the wings (eg BD+40°4124, M17SW IRS and VV Ser), or else returned values that indicate that although the profile can be a good match, the estimated parameters are not physically sensible (eg MWC 297). It may be that the success of this model in the case of Lk H $\alpha$  101 by Hamman and Persson (1989) was fortuitous, since it is a very similar type of object. They

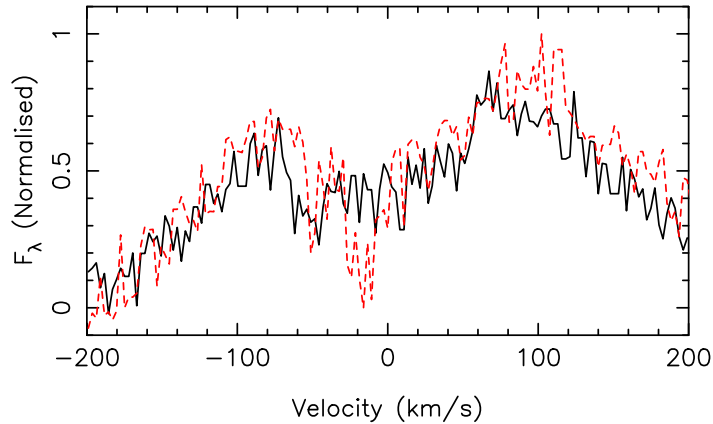


**Figure 7.** The profiles of the FeII 1.688 $\mu$ m line in S106 IRS separated by 378 days. The first epoch is the solid line.

fitted to H $\alpha$  which will have more easily detectable wings for electron scattering, and hence they can be seen to higher velocities which is what drives the fit to the electron temperature. It is worth considering briefly why the model fits at all if the parameter estimation is so poor. The reason is simply that outlined by Laor (2006) – multiple scattering gives rise to a close to exponential profile, and the high velocity component of the Castor et al model is essentially very close to an exponential. It seems clear that a full Monte-Carlo approach to modelling these systems, such as that outlined in Kurosawa et al. (2011), is required to proceed much further with any analysis.

We have also shown that the 1.688 $\mu$ m  $z^4F_9$ – $c^4F_9$  FeII line is seen in massive and intermediate mass young stellar objects. We have successfully modelled this line with a simple Keplerian disc in all sources bar S106 IRS. The model results are largely in agreement with those found from interferometric near and mid infrared measurements of the continuum where such data exist. We therefore ascribe a disc origin to the FeII line in most sources, since we know from the interferometry and other data that these sources do have discs, and our simple model fits are largely successful. This is in agreement with previous findings from optical data that fluorescent FeII emission is a good disc tracer in classical Be stars. The counter-example of S106 IRS cautions against too simple an over-interpretation of this result however.

Overall therefore, these data are strongly suggestive that all of the sources observed have evidence that a disc is present, as expected for such young sources, and the line broadening indicates a very dense circumstellar environment. The likeliest origin for the bulk of the emission lines is a combination of a disc and a wide opening angle wind or disc-wind. The relative contributions of the latter varies widely between different species and even different lines of the same species. The similarity of features between these sources and lower mass T Tauri stars is notable.

## 5 ACKNOWLEDGMENTS

We are grateful to the referee Juan Zorec for his very helpful referee’s report. The United Kingdom Infrared Telescope is operated by the Joint Astronomy Centre on behalf of the Science and Technology Facilities Council of the U.K. HEW acknowledges support from STFC through a studentship and as a postdoctoral research associate.

## REFERENCES

- Acke, B. et al., 2008, *A&A*, 485, 209
- Alonso-Albi, T., Fuente, A., Bachiller, R., Neri, R., Planesas, P., Testi, L., Berné, O., Joblin, C., 2009, *A&A*, 497, 117
- Arias M.L., Zorec J., Cidale L., Ringuet A.E., Morrell N.I., Ballereau D., 2006, *A&A*, 460, 821
- Baldwin, J.A., Ferland, G.J., Korista, K.T., Hamann, F., LaCluyzé, A., 2004, *ApJ*, 615, 610
- Bik, A., Thi, W.F., 2004, *A&A*, 427, L13
- Blake, G.A., Boogert, A.C.A., 2004, *ApJ*, 606, L73
- Blum, R.D., Barbosa, C.L., Damineli, A., Conti, P.S., Ridgway, S., 2004, *ApJ*, 617, 1167
- Bonnell, I.A., Vine, S.G., Bate, M.R., 2004, *MNRAS*, 349, 735
- Bunn, J.C., Hoare, M.G., Drew, J.E., 1995, *MNRAS*, 272, 346
- Campbell, B., Persson, S.E., McGregor, P.J., 1986, *ApJ*, 305, 336
- Canto, J., Rodriguez, L.F., Calvet, N., Levreault, R.M., 1984, *ApJ*, 282, 631
- Carciofi, A.C., Bjorkman, J.E., 2006, *ApJ*, 639, 1081
- Carciofi, A.C., Domiciano de Souza, A., Magalhães, A.M., Bjorkman, J.E., Vakili, F., 2008, *ApJ*, L41
- Cardelli, J.A., Clayton, G.C., Mathis, J.S., 1989, *ApJ*, 345, 245
- Carr, J.S., 1989, *ApJ*, 345, 522
- Castor, J.I., Smith, L.F., van Blerkom, D., 1970, 159, 1119

- Chandler, C.J., Carlstrom, J.E., Scoville, N.Z., 1995, *ApJ*, 446, 793
- Chini, R., Hoffmeister, V.H., Kämpgen, K., Kimeswenger, S., Nielbock, M., Siebenmorgen, R., 2004, *A&A*, 427, 849
- Cohen, M., Bieging, J.H., Welch, W.J., Dreher, J.W., 1985, *ApJ*, 292, 249
- Corcoran, M., Ray, T.P., 1997, *A&A*, 321, 189
- Crowther, P.A., 2005, in Cesaroni, R., Felli, M., Churchwell, E., Walmsley, M., eds, *IAU Symp. 227, "Massive Star Birth: A Crossroads of Astrophysics"*, p. 389
- Danchi, W.C., Tuthill, P.G., Monnier, J.D., 2001, *ApJ*, 562, 440
- Davies B., Lumsden S.L., Hoare M.G., Oudmaijer R.D., de Wit W.-J., 2010, *MNRAS*, 402, 1504
- de Wit W.J., Hoare M.G., Oudmaijer R.D., Nürnberger D.E.A., Wheelwright H.E., Lumsden S.L., 2011, *A&A*, 526, L5
- Drew, J.E., Bunn, J.C., Hoare, M.G., 1993, *MNRAS*, 265, 12
- Drew, J.E., Busfield, G., Hoare, M.G., Murdoch, K.A., Nixon, C.A., Oudmaijer, R.D., 1997, *MNRAS*, 286, 538
- Edwards, S., Fischer, W., Hillenbrand, L., Kwan, J. 2006, *ApJ*, 646, 319
- Eisner, J.A., Lane, B.F., Akeson, R.L., Hillenbrand, L.A., Sargent, A.I., 2003, *ApJ*, 588, 360
- Eisner, J.A., Lane, B.F., Hillenbrand, L.A., Akeson, R.L., Sargent, A.I., 2004, *ApJ*, 613, 1049
- Felli, M., Massi, M., Staude, H.J., Reddmann, T., Eiroa, C., Hefele, H., Neckel, T., Panagia, N., 1984, *A&A*, 135, 261
- Folha, D.F.M., Emerson, J.P. 2001, *A&A*, 365, 90
- Follert, R., Linz, H., Stecklum, B., van Boekel, R., Henning, T., Feldt, M., Herbst, T. M., & Leinert, C., 2010, in press
- Fuente, A., Martin-Pintado, J., Bachiller, R., Cernicharo, J. 1990, *A&A*, 237, 471
- Gordon, M.A., 2003, *ApJ*, 589, 953
- Gordon, M.A., Holder, B.P., Jisonna, L.J., Jr., Jorgenson, R.A., Strelitski, V.S. 2001, *ApJ*, 559, 402
- Hamann, F., Simon, M., 1986, *ApJ*, 311, 909
- Hamann, F., Simon, M., 1988, *ApJ*, 339, 1078
- Hamann, F., Persson, S.E., 1989, *ApJS*, 71, 931
- Hamann, F., Persson, S.E., 1992, *ApJS*, 82, 285
- Hamann, F., Depoy, D.L., Johansson, S., Elias, J., 1994, *ApJ*, 422, 626
- Hanson, M.M., Howarth, I.D., Conti, P.S., 1997, *ApJ*, 489, 698
- Hanson, M.M., Kudritzki, R.-P., Kenworthy, M.A., Puls, J., Tokunaga, A.T. 2005, *ApJS*, 161, 154
- Harmanec, P., 1988, *Bull. Astron. Inst. Czechoslovakia*, 39, 329
- Hernández, J., Calvet, N., Briceño, C., Hartmann, L., Berlind, P., 2004, *AJ*, 127, 1682
- Hinkle, K., Wallace, L., Livingston, W., 1995, *PASP*, 107, 1042
- Hippelein, H., Muench, G., 1981, *A&A*, 99, 248
- Hoare, M.G., 2006, *ApJ*, 649, 856
- Hofmann, K.-H., Balega, Y., Ikhsanov, N.R., Miroshnichenko, A.S., Weigelt, G., 2002, *A&A*, 395, 891
- Hoffmeister, V.H., Chini, R., Scheyda, C.M., Schulze, D., Watermann, R., Nürnberger, D., Vogt, N. 2008, *ApJ*, 686, 310
- Hollenbach, D., Johnstone, D., Lizano, S., Shu, F., 1994, *ApJ*, 428, 654
- Hosokawa T., Omukai K., 2009, *ApJ*, 691, 823
- Johansson, S., 1978, *Phys. Scr.* 18, 217
- Johansson, S., Letokhov, V.S., 2007, *NewAR*, 51, 443
- Kahn, F.D., 1974, *A&A*, 37, 149
- Kelly, D.M., Rieke, G.H., Campbell, B., 1994, *ApJ*, 425, 231
- Kleinmann, D.E., & Wright, E.L., 1973, *ApJ*, 185, L131
- Kraus, M., Krügel, E., Thum, C., Geballe, T.R., 2000, *A&A*, 362, 158
- Kraus S., et al., 2010, *Natur*, 466, 339
- Krumholz, M.R., Klein, R.I., McKee, C.F., Offner, S.S.R., & Cunningham, A.J., 2009, *Science*, 323, 754
- Kuiper, R., Klahr, H., Beuther, H., Henning, T., 2010, *ApJ*, 722, 1556
- Kurosawa R., Romanova M.M., Harries T.J., 2011, *MNRAS*, 416, 2623
- Lada, C.J., 1976, *ApJS*, 32, 603
- Laor, A., 2006, *ApJ*, 643, 112
- Lenorzer, A., de Koter, A., Waters, L.B.F.M., 2002, *A&A*, 386, L5
- Linz, H. et al. 2009, *A&A*, 505, 655
- Lumsden, S.L., Puxley, P.J., 1996, *MNRAS*, 281, 493
- Malbet, F. et al., 2007, *A&A*, 464, 43
- McKee, C.F., Tan, J.C., 2003, *ApJ*, 585, 850
- Meléndez, J., Barbuy, B., 1999, *ApJS*, 124, 527
- Meyer, J.M., Nordsieck, K.H., Hoffman, J.L., 2002, *AJ*, 123, 1639
- Montesinos, B., Eiroa, C., Mora, A., Merín, B. 2009, *A&A*, 495, 901
- Murdoch, K.A., Drew, J.E. 1994, in The, P.S., Perez, M.R., Van den Heuvel, E.P.J., eds, *ASP Conf. Series* 62, "The Nature and Evolutionary Status of Herbig Ae/Be Stars", p. 377
- Muzerolle, J., Calvet, N., Hartmann, L. 2001, *ApJ*, 550, 944
- Oudmaijer, R.D., 1998, *A&AS*, 129, 541
- Oudmaijer, R.D., Busfield, G., Drew, J.E., 1997, *MNRAS*, 291, 797
- Oudmaijer, R.D., Drew, J.E., 1999, *MNRAS*, 305, 166
- Oudmaijer, R.D., Drew, J.E., Vink, J.S., 2005, *MNRAS*, 364, 725
- Oudmaijer, R.D. et al. 2011, *Astronomische Nachrichten*, 332, 238
- Persson, S.E., Geballe, T.R., McGregor, P.J., Edwards, S., Lonsdale, C.J., 1984, *ApJ*, 286, 289
- Pontoppidan, K.M., Dullemond, C.P., Blake, G.A., Evans, N.J., II, Geers, V.C., Harvey, P.M., Spiesman, W., 2007, *ApJ*, 656, 991
- Pontoppidan, K.M., Blake, G.A., Smette, A. 2011, *ApJ*, 733, 84
- Porter, J.M., Drew, J.E., Lumsden, S.L. 1998, *A&A*, 332, 999
- Pringle, J.E., 1981, *ARA&A*, 19, 137
- Prisinzano, L., Damiani, F., Micela, G., Sciortino, S., 2005, *A&A*, 430, 941
- Ramsauer J., Solanki S.K., Biemont E., 1995, *A&AS*, 113, 71
- Reipurth, B., Pedrosa, A., Lago, M.T.V.T., 1996, *A&AS*, 120, 229

- Repolust T., Puls J., Hanson M.M., Kudritzki R.-P., Mokiem M.R., 2005, *A&A*, 440, 261
- Quirrenbach, A., Albrecht, S., Tubbs, R.N., 2006, Kraus, M., Miroshnichenko, A.S., eds, ASP Conference Series, Vol. 355, “Stars with the B[e] Phenomenon”, p.239
- Saito, H. et al., 2009, *AJ*, 137, 3149
- Schneider, N., Simon, R., Bontemps, S., Comerón, F., Motte, F., 2007, *A&A*, 474, 873
- Schreyer, K., Henning, T., van der Tak, F.F.S., Boonman, A.M.S., van Dishoeck, E.F., 2002, *A&A*, 394, 561
- Schreyer, K., Semenov, D., Henning, T., Forbrich, J., 2006, *ApJ*, 637, L129
- Shu, F.H., Adams, F.C., Lizano, S., 1987, *ARA&A*, 25, 23
- Sim, S.A., Drew, J.E., Long, K.S., 2005, *MNRAS*, 363, 615
- Simon, M., Cassar, L., Felli, M., Fischer, J., Massi, M., Sanders, D., 1984, *ApJ*, 278, 170
- Solf, J., Carsenty, U., 1982, *A&A*, 113, 142
- Stahler, S.W., Palla, F., Ho, P.T.P., 2000, Mannings, V., Boss, A.P., Russell, S.S., eds, *Protostars and Planets IV*, p.327
- Storey, P.J., Hummer, D.G. 1995, *MNRAS*, 272, 41
- Thum, C., Matthews, H.E., Martin-Pintado, J., Serabyn, E., Planesas, P., Bachiller, R., 1994, *A&A*, 283, 582
- Thronson, H.A., Jr., Loewenstein, R.F., Stokes, G.M., 1979, *AJ*, 84, 1328
- Vakili, F. et al., 1998, *A&A*, 335, 261
- van den Ancker, M.E., de Winter, D., Tjin A Djie, H.R.E., 1998, *A&A*, 330, 145
- van den Ancker, M.E., Wesselius, P.R., Tielens, A.G.G.M., 2000, *A&A*, 355, 194
- Vink, J.S., Drew, J.E., Harries, T.J., Oudmaijer, R.D., 2002, *MNRAS*, 337, 356
- Vink, J.S., Drew, J.E., Harries, T.J., Oudmaijer, R.D., Unruh, Y., 2005, *MNRAS*, 359, 1049
- Weigelt, G., et al. 2011, *A&A*, 527, A103
- Weintroub, J., Moran, J.M., Wilner, D.J., Young, K., Rao, R., Shinnaga, H., 2008, *ApJ*, 677, 1140
- Wheelwright, H.E., Oudmaijer, R.D., de Wit, W.J., Hoare, M.G., Lumsden, S.L., Urquhart, J.S., 2010, *MNRAS*, 408, 1840
- Willner, S.P. et al., 1982, *ApJ*, 253, 174
- Wouterloot, J.G.A., Brand, J., 1989, *A&AS*, 80, 149
- Zorec, J., Arias, M.L., Cidale, L., Ringuelet, A.E., 2007, *A&A*, 470, 239